AD-A092 956 NAVAL RESEARCH LAB WASHINGTON DC F/G 20/5
THEORY OF THE QUASI-OPTICAL ELECTRON CYCLOTRON MASER.(U)
DEC 80 P SPRANGLE, J L VOMVORIDIS
UNCLASSIFIED NRL-MR-4366 NL

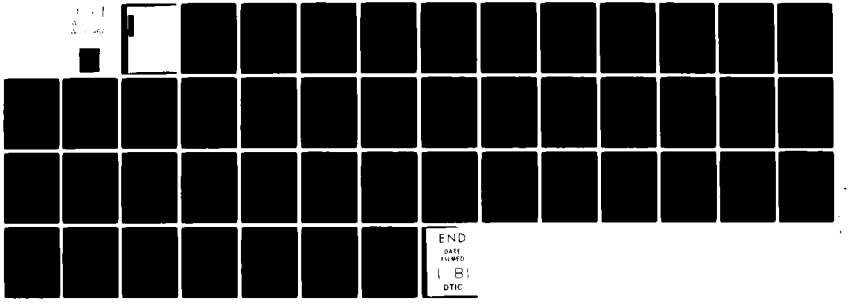

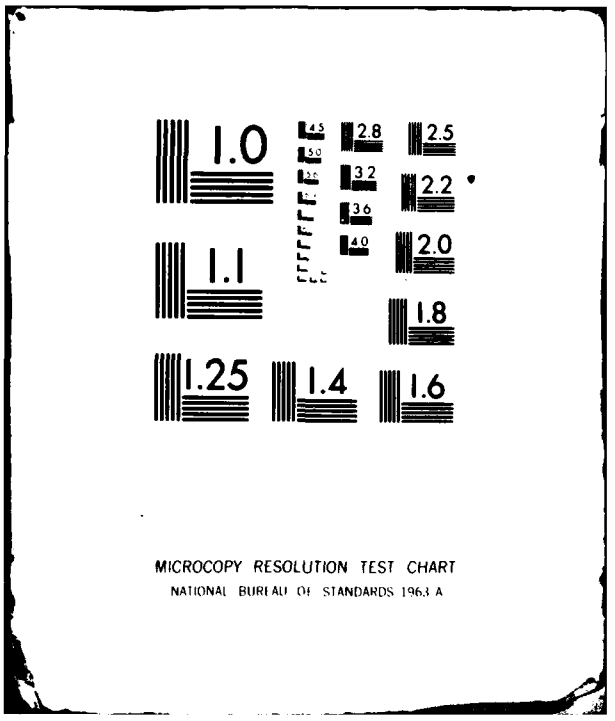
1.0
1.1
1.25
1.4
1.6
1.8
2.0
2.2
2.5
2.8
3.2
3.6
4.0
MICROCOPY RESOLUTION TEST CHART
NATIONAL BUREAU OF STANDARDS 1963 A

(14) NRL-MR-4366

SECURITY CLASSIFICATION OF THIS PAGE (When Data Entered)

(16) RR011109

(9) REPORT DOCUMENTATION PAGE

READ INSTRUCTIONS BEFORE COMPLETING FORM

1. REPORT NUMBER: NRL Memorandum Report 4366	2. GOVT ACCESSION NO.: AD-A092956
3. RECIPIENT'S CATALOG NUMBER:	
4. TITLE (and Subtitle): (6) THEORY OF THE QUASI-OPTICAL ELECTRON CYCLOTRON MASER	5. TYPE OF REPORT & PERIOD COVERED: Interim report on a continuing problem.
	6. PERFORMING ORG. REPORT NUMBER:
7. AUTHOR(s): (10) P. Sprangle, J.L. Vomvoridis* and W.M. Manheimer	8. CONTRACT OR GRANT NUMBER(s):
9. PERFORMING ORGANIZATION NAME AND ADDRESS: Naval Research Laboratory, Washington, D.C. 20375	10. PROGRAM ELEMENT, PROJECT, TASK AREA & WORK UNIT NUMBERS: (17) 61153N 11; RR011 09 41; 67-0899-0-0
11. CONTROLLING OFFICE NAME AND ADDRESS: Office of Naval Research, Arlington, VA 22209 (11) (12)	12. REPORT DATE: December 9, 1980
	13. NUMBER OF PAGES: 46
14. MONITORING AGENCY NAME & ADDRESS (if different from Controlling Office): (12) 47	15. SECURITY CLASS. (of this report): UNCLASSIFIED
	15a. DECLASSIFICATION/DOWNGRADING SCHEDULE:

16. DISTRIBUTION STATEMENT (of this Report)

Approved for public release; distribution unlimited.

17. DISTRIBUTION STATEMENT (of the abstract entered in Block 20, if different from Report)

18. SUPPLEMENTARY NOTES

*JAYCOR, Alexandria, VA 22304

19. KEY WORDS (Continue on reverse side if necessary and identify by block number)

Electron cyclotron maser
Quasi-optical
Open resonator
Ultra-high-power-source

20. ABSTRACT (Continue on reverse side if necessary and identify by block number)

In this work a promising new electron cyclotron maser oscillator is proposed and analyzed. The configuration utilizes an open resonator cavity containing a gyrating electron beam which translates along an external magnetic field. The magnetic field is directed perpendicular to the axis of symmetry of the open resonator. Because the wave-particle interaction volume is extremely large, the total input electron beam power can be high and the power density low.

(Continues)

DD FORM 1 JAN 73 1473 EDITION OF 1 NOV 65 IS OBSOLETE
S/N 0102-LF-014-6601

251950

SECURITY CLASSIFICATION OF THIS PAGE (When Data Entered)

20. Abstract (Continued)

This configuration has a number of potentially very attractive features. Among them are: i) high operating radiation power levels (> MWs), ii) high efficiency operation (> 45%), iii) naturally suited to short wavelength operation (λ<2mm), iv) operates efficiently at low electron beam voltage (10-100 keV), v) natural transverse mode selectivity, vi) moderate insensitivity to beam temperature effects. The non-linear interaction between the electrons and resonator field have been analyzed and an expression for the steady state efficiency obtained.

The expression for efficiency has a rather simple analytic form when the amplitude of the resonator fields are small, i.e., small signal regime. In this case, the efficiency is an essentially odd, non-oscillating function of the frequency mismatch (difference between resonator frequency and relativistic cyclotron frequency).

For a uniform external magnetic field, total efficiencies in excess of 30% can be realized. We have considered enhancing the efficiencies by spatially contouring the magnetic field. Appropriately contouring the magnetic field across the resonator by ~ 5% increases the efficiency from ~ 35% to ~ 45%.

CONTENTS

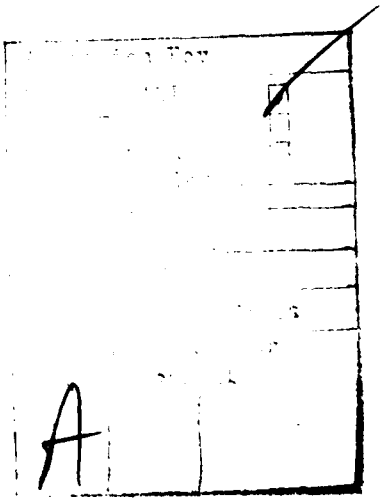

THEORY OF THE QUASI-OPTICAL ELECTRON CYCLOTRON MASER

I. INTRODUCTION

At the present time, two classical radiation mechanisms, i.e., the free electron laser[1-9] (FEL) and electron cyclotron maser[10-19] (ECM), are under extensive study because of the great potential they show as new classes of coherent radiation sources. Experimental results on the FEL[20-22] and ECM[22-25] have been very encouraging.

In free electron lasers the active medium is a beam of relativistic electrons. Such sources have the potential for generating coherent radiation ranging from the millimeter to the optical regime and beyond. They are frequency tunable and in principle extremely efficient generators of intense radiation.

The electron cyclotron maser in its present form has reached a far more mature stage of development than the FEL. In the millimeter regime, electron cyclotron masers have generated power levels substantially higher and more efficiently than the more conventional radiation sources. Experimental efficiencies are impressive, e.g., 22% efficiency at λ = 2mm with a CW output power of 22 kW.[23]

In this paper we propose and analyze a new electron cyclotron maser oscillator configuration, which utilizes an open resonator cavity. Our quasi-optical cyclotron maser has a unique potential for becoming a new type of coherent radiation source. In principle, the device is capable of generating coherent radiation in the millimeter to submillimeter regime,

Manuscript submitted October 6, 1980.

at power levels in excess of magawatts, with efficiencies exceeding 50%. The basic structure consists of an open resonator containing a beam of electrons gyrating about, as well as streaming parallel to, an applied magnetic field. The magnetic field is directed transverse to the axis of the open resonator, which consists of two or more appropriately curved mirrors. Moderately low electron beam energies can be used, i.e., 10-100 keV, even though the wave-particle interaction mechanism is due to relativistic effects. This configuration has a number of distinct advantages over the more conventional radiation sources. Some of these advantages are: i) extremely high operating power levels, ii) high operating frequency, iii) high efficiency and, iv) natural transverse mode selection. Since we utilize an open resonator and, thus, have a large interaction volume, the input electron beam power can be extremely high while the power density can be kept moderately low. The usual limitations on beam power imposed by space charge effects can therefore be overcome. Since the wave-particle interaction is fairly efficient (~50%), high radiation power levels can be achieved. The operating frequency is limited solely by the external magnetic field and is independent of the dimensions of any physical structure. Favorable coupling between the electrons and radiation field occurs near harmonics of the relativistic cyclotron frequency.

A quasi-optical resonator has many modes which in principle can experience gain, producing a multi-mode output signal. The fundamental transverse resonator mode can be preferentially excited in the open resonator. If the mirrors in the open resonator are made large enough to intercept a large fraction of the flux in the fundamental mode, we may expect this mode to have a large Q. The higher order modes can be expected to have a substantially smaller Q since they suffer from diffraction losses. This

is an advantage over a closed cavity, where all modes would have comparable values of Q. Longitudinal modes in resonance within the resonator can undergo gain and produce a multi-mode output signal, unless they are suppressed. Longitudinal mode selection can be achieved by employing a mode selection; one such selector is the Smith-Fox interferometer.[26]

This new maser configuration, like the conventional electron cyclotron maser (gyrotron), has a wide range of practical applications. These applications range from electron cyclotron heating of fusion plasmas to advanced radar and communications systems. Because of the high field level, short wavelength and extended interaction volume, the quasi-optical maser may be a natural electro-magnetic pump source for a free electron laser. In this application a second highly relativistic electron beam propagating along the axis of the open resonator would interact with the resonator field and induce high frequency radiation. The frequency of the scattered radiation would be $\sim 4\gamma_y^2\omega$, where γ_y is the longitudinal gamma factor of the second relativistic electron beam and ω is the frequency of the quasi-optical maser.

II. NON-LINEAR ANALYSIS OF QUASI-OPTICAL MASER

The quasi-optical cyclotron maser configuration is depicted in Figure 1. The lowest order mode is the well known TEM_{oo} Gaussian radiation beam, see Figure 2. For the electric field vector primarily polarized in the x direction, the field components of this mode are

$$E_x(x,y,z,t) = E\,(x,y,z) \sin\,(k_y y + \alpha(x,y,z)) \cos \omega t, \tag{1a}$$

$$B_z(s,y,z,t) = E\,(x,y,z) \cos\,(k_y y + \alpha(x,y,z)) \sin \omega t, \tag{1b}$$

where $k_y=\omega/c$, $E(x,y,z)=E_o(r_o/r_s(y))\exp(-(x^2+z^2)/r^2_s(y))$, $\alpha(x,y,z)=$

$R^{-1}(y)(x^2+z^2)(\omega/c)/2 \; - \tan^{-1}(y/y_R)$,

ω is the radiation frequency, E_o is the field amplitude at the origin, r_o is the minimum spot size at the plane y=0, $r_s(y) = r_o\,(1+y^2/y_R^2\,)^{1/2}$ is the spot size at the plane y, $y_R = r_o^2\omega/2c$ is the Rayleigh length and $R(y) = y(1+y_R^2/y^2)$ is the radius of curvature of the spherical wavefront at y. The y components of the field are $E_y = -\,(c/\omega)\,\partial\, E_x/\,\partial x$ and $B_y = -\,(c/\omega)\,\partial B_z/\,\partial z$. Note that $|E_y|, |B_y| \ll |E_x|, |B_z|$. One can show that the $\underset{\sim}{E}$ and $\underset{\sim}{B}$ fields satisfy the appropriate boundary conditions on the mirror. This is equivalent to saying that the mirror radius of curvature equals the wavefront radius of curvature.

The intermode frequency spacing is $\delta\omega = \pi c/L$ where L is the separation between the mirrors and the diffraction angle of the radiation is $\Theta_d = \lambda/\pi r_o$ where $\lambda = 2\,\pi c/\omega$ is the radiation wavelength.

Other orientations of the external magnetic field and, hence, the gyrating electric beam are possible. Careful analysis, however, shows that these other configurations may not be as straightforward to implement.

For example, another possible configuration is where the magnetic field and the streaming electrons are directed along the y axis. It can be shown that to maintain wave-particle coherence the thermal spread in the y component of electron velocity must satisfy $\delta v_y/v_y \ll \lambda/2\pi L$. For long resonators this condition places a rather stringent requirement on the electron beam quality.

In Figure 1, the gyrating beam electrons rotate in the x-y plane and stream along the external magnetic field $\underset{\sim}{B}_0$ which is directed along the z axis. For convenience we locate the sheet electron beam of width L_b on the y-z plane,as shown in Figure 1. Furthermore, for reasons of analytic simplicity,we take the guiding centers of the electrons, upon entering the resonator fields, to lie on the y-z plane. Also the electrons, upon entering the resonator, are assumed to have the same transverse and parallel velocities.

Strong coupling between the electrons and resonator field will occur at frequencies near multiples of the relativistic electron cyclotron frequency. Let us consider the fundamental cyclotron interaction, $\omega \approx \Omega_0/\gamma$ where $\Omega_0 = |e|B_0/m_0 c$, $\gamma = (1+\underset{\sim}{p}\cdot\underset{\sim}{p}/m_0^2c^2)^{\frac{1}{2}}$ and $\underset{\sim}{p}$ is the electron momentum vector. The electron Larmor radius is in general much less than the radiation wavelength, i.e., $r_L = \gamma v_\perp/\Omega_0 = \beta_\perp \lambda/2\pi \ll \lambda$, where $v_\perp = c\beta_\perp$ is the transverse electron velocity. The minimum radiation spot size is much greater than the Larmor radius, $r_0 > \lambda \gg r_L$. Therefore, by choosing the width of the electron beam to be somewhat less than the Rayleigh length, $L_b < y_R$, the resonator fields in (1) felt by the electrons can be accurately approximated by the plane wave fields,

$$E_x(y,z,t) = E(z) \sin\left(\frac{\omega}{c}y\right) \cos(\omega t) , \tag{2a}$$

$$B_y(y,z,t) = E(z) \cos\left(\frac{\omega}{c}y\right) \sin(\omega t) , \tag{2b}$$

where $E(z) = E_0 \exp(-z^2/r_0^2)$ and $E_y = B_y \approx 0$.

We now express the particle momenta $\underline{p}$ and transverse position (x,y) as functions of Lagrangian independent variables. In general, a convenient set of Lagrangian independent variables for this problem are the z position of the particles, the initial momentum space angle Θ_0, initial transverse coordinates of the guiding center x_{go} and y_{go} and the particle entrance time into the resonator field t_0. Since the resonator fields fall off like $\exp(-z^2/r_0^2)$, the entrance position of the sheet beam z_{in} can be taken to be a few spot sizes away from the y axis, $|z_{in}| >> r_0$. In our present analysis, $x_{go} = 0$, $|y_{go}| \leq L_b$ and t_0 is the time the particle crosses the $z = z_{in}$ plane. The functional dependence of the particle momenta vector and transverse coordinates is $\underline{p} = \underline{p}(z,y_{go},\Theta_0,t_0)$, $x = x(z,y_{go},\Theta_0,t_0)$ and $y = y(z,y_{go},\Theta_0,t_0)$.

The orbit equations for the electrons are

$$p_z \frac{dp_y}{dz} = - |e| (\gamma m_0 E_x + p_y(B_0+B_z)/c), \tag{3a}$$

$$p_z \frac{dp_y}{dz} = |e| p_x (B_0+B_z)/c , \tag{3b}$$

$$\frac{dp_z}{dz} = 0 , \tag{3c}$$

where the fields E_x and B_z are given by (2), with t replaced by the Lagrangian time variable $\tau(z, y_{go}, \Theta_0, t_0) = t_0 + \int_{z_{in}}^{z} dz'/v_z$ and $v_z = p_z(z,y_{go},\Theta_0,t_0)/\gamma(z,y_{go},\Theta_0,t_0)\, m_0$ is the longitudinal particle velocity.

Note that p_z is a constant of the motion denoted by p_{zo}, hence, $v_z \neq 0$ unless $p_{zo} = 0$. The Lagrangian time variable, τ, is the time it takes a particle to arrive at z if it crossed the $z=z_{in}$ plane at time t_o with a momentum space angle Θ_o and guiding center position ($x_{go}=0$, $y_{go}=0$). Since we are considering only the fundamental cyclotron interaction, an appropriate representation of the solutions of the orbit equations in (3) are

$$p_x(z) = p_{xg}(z) + p_\perp(z) \cos(\omega\tau+\Theta), \tag{4a}$$

$$p_y(z) = p_{yg}(z) + p_\perp(z) \sin(\omega\tau+\Theta), \tag{4b}$$

where p_{xg},p_{yg} are the components of momenta associated with the guiding centers, $p_\perp$ is the transverse particle momentum and $\omega\tau+\Theta$ is the particle momentum space angle. In (4) the dependent variables p_{xg},p_{yg}, $p_\perp$, and Θ are assumed to be slowly varying functions of z as well as functions of y_{go}, Θ_o and t_o. By "slowly varying" we mean that the quantity has no high (cyclotron) frequency Fourier components. The variables p_{xg},p_{yg}, $p_\perp$ and Θ are not functionally independent of each other. In fact, by requiring that they be slowly varying functions of z, we will derive four separate but coupled equations which uniquely determine them. The field amplitude E(z) defined in Eq (2), denotes the profile of the radiation beam and is a slowly varying function of z since the electrons undergo many cyclotron orbits while traversing the resonator fields. The initial values of dependent variables upon entering the open resonator fields are $p_{xg}(z=z_{in}) = p_{yg}(z=z_{in}) = 0$, $p_\perp(z=z_{in}) = p_{\perp o}$, $v_z(z=z_{in})=v_{zo}=p_{zo}/\gamma_o m_o$ and $\Theta(z=z_{in}) = \Theta_o$. Furthermore, it will be shown that the guiding center drift momentum of the particles is much less than the transverse momentum, i.e., $|p_{xg}|,|p_{yg}| \ll p_\perp$. Noting the form for p_y in (4b), we see that the

dependent variable y can be approximated by

$$y = y_g - \frac{p_\perp}{m_o \Omega_o} \cos(\omega\tau+\Theta), \tag{5}$$

where y_g is the slowly varying y position of the guiding center, hence, $p_{yg} = p_{z0}\, dy_g/dz$ and $p_\perp/m_o\Omega_o = r_L$ is the electron Larmor radius.

We now substitute (4a,b) together with (5) into the orbit equations (3a,b) and carry out the appropriate operations. Keeping in mind that E(z) is a slowly varying function of z we equate rapidly varying terms and slowly varying terms and discard all frequencies of order $2\Omega_o$. These manipulations yield four interrelated self-consistent non-linear equations describing the spatial evolution of $p_\perp$, Θ, p_{xg} and p_{yg}, When $r_L \ll \lambda$, these equations are

$$\frac{dp_\perp}{dz} = -\frac{|e|E\gamma m_o}{2p_{zo}} \left[\sin\left(\frac{\omega}{c} y_g\right) \cos\Theta + \cos\left(\frac{\omega}{c} y_g\right)\left(\frac{p_{xg}}{m_o c} \cos\Theta + \frac{p_{yg}}{m_o c} \sin\Theta\right)\right], \tag{6a}$$

$$\frac{d\Theta}{dz} = (\Omega_o - \gamma\omega)\, m_o/p_{zo} + \frac{|e|E\gamma m_o}{2p_{zo}p_\perp}\left[\sin\left(\frac{\omega}{c} y_g\right) \sin\Theta - \cos\left(\frac{\omega}{c} y_g\right) \left(\frac{p_{xg}}{m_o c} \sin\Theta - \frac{p_{yg}}{m_o c} \cos\Theta\right)\right], \tag{6b}$$

$$p_{xg} = \frac{|e|E\, p_\perp}{2\Omega_o m_o c} \cos\left(\frac{\omega}{c} y_g\right) \sin\Theta \quad , \tag{6c}$$

$$p_{yg} = -\frac{|e|Ep_\perp}{2\Omega_o m_o c} \left(1 - \frac{\omega\gamma}{\Omega_o}\right) \cos\left(\frac{\omega}{c} y_g\right) \cos\Theta \ , \tag{6d}$$

where $dy_g/dz = p_{yg}/p_{zo}$ and $\gamma = (1+(p_{zo}^2 + p_\perp^2)/m_o^2c^2)^{\frac{1}{2}}$. Equations (6) completely describe the non-linear steady state particle dynamics for the fundamental cyclotron interaction. Since $|E/B_o| \ll 1$, it is noted from (6c)

and (6d) that $|p_{xg}|, |p_{yg}| << p_\perp$, justifying the corresponding earlier assumption. The trajectory of each electron is described by the set of equations in (6). The initial conditions, however, are different for each electron, as required by the input distribution. For an entering cold unbounded electron beam, the initial conditions are such that at $z=z_{in}$, $p_{xg}=0$, $p_{yg}=0$, $p_\perp = p_{\perp o}$, $p_z=p_{zo}$, $\Theta=\Theta_o$ where Θ_o ranges from 0 to 2π and $y_g=y_{go}$ where y_{go} ranges from $-L_b/2$ to $L_b/2$, while $p_{\perp o}$ and p_{zo} are the same for all electrons.

The equations in (6) can be considerably simplified by noting from (6c,d) that $p_{xg}/m_o c \simeq O(\gamma v_\perp E/2B_o) << 1$ and $p_{yg}/m_o c \approx 0$ $(p_{xg}\Delta\omega/m_o c\omega)$. Hence, the second and third terms in the brackets on the right hand side of (6a,b) can be neglected and y_g in (6a,b) can be replaced by y_{go}. The resulting equations are

$$\frac{dp_\perp}{dz} = -\frac{|e|E\gamma m_o}{2p_{zo}} \sin\left(\frac{\omega}{c} y_{go}\right) \cos\Theta \,, \tag{7a}$$

$$\frac{d\Theta}{dz} = (\Omega_o - \gamma\omega)\, m_o/p_{zo} + \frac{|e|E\gamma m_o}{2p_{zo}p_\perp} \sin\left(\frac{\omega}{c} y_{go}\right) \sin\Theta. \tag{7b}$$

These equations are very similar to those analyzed in our initial studies of the non-linear behavior of the cyclotron maser instability.

In a temporal steady state oscillator the efficiency of converting beam power to radiation power is given by

$$\eta = (P_{b,in} - P_{b,out})/P_{b,in} \tag{8}$$

where $P_{b,in}$ and $P_{b,out}$ is the total electron beam power flowing into and out of the open resonator in the z direction. For the cold beam distribution presented earlier, the efficiency, as defined in (8), can

be shown to give

$$\eta = \frac{-|e|}{\gamma_o(\gamma_o-1)v_{zo}m_o^2c^2} \int_{z=z_{in}}^{z=z_{out}} dz \int_0^{2\pi/\omega} \frac{dt_o}{2\pi/\omega} \int_{-L_b/2}^{L_b/2} \frac{dy_{go}}{L_b} \int_0^{2\pi} \frac{d\Theta_o}{2\pi} E_x p_x \ . \quad (9)$$

Using (2a) and (4a) we find that

$$E_x p_x = \frac{E\, p_\perp}{2} \sin\left(\frac{\omega}{c} y_{go}\right) \cos\Theta \ , \quad (10)$$

where we have used the approximations $y \approx y_{go}$ and $p_{xg} \simeq 0$. Substituting (10) into (9) and noting that $E_x p_x$ is independent of t_o we obtain for the efficiency the expression

$$\eta = \frac{-|e|\ \omega}{4\pi\gamma_o(\gamma_o-1)v_{zo}m_o^2c^2} \int_{z=z_{in}}^{z=z_{out}} dz \int_{-L_b/2}^{L_b/2} \frac{dy_{go}}{L_b}$$

$$\int_0^{2\pi} \frac{d\Theta_o}{2\pi} E(z)\, \underline{P}(z,\Theta_o,y_{go}) \sin\left(\frac{\omega}{c} y_{go}\right) \cos\Theta(z,\Theta_o,y_{go}). \quad (11)$$

The expression in (11) gives the full non-linear steady state operating efficiency. Before solving (11) in the fully non-linear regime it is illuminating to first solve the orbit equations in the linear regime and thereby obtain the analytic form for the efficiency. The orbit equation in (7) can be linearized by setting $p_\perp = p_\perp^{(0)} + p_\perp^{(1)}$ and $\Theta = \Theta^{(0)} + \Theta^{(1)}$, where $p_\perp^{(0)}$ and $\Theta^{(1)}$ are zero order quantities in the field amplitude, E, and $p_\perp^{(1)}$ and $\Theta^{(1)}$ are first order quantities. Solving (7) we find that

$$p_\perp^{(0)} = p_{\perp o} \ , \quad (12a)$$

$$\Theta^{(0)}(z) = \Theta_o - \frac{\Delta\omega}{v_{zo}} (z - z_{in}), \quad (12b)$$

$$p_{\perp}^{(1)} = \frac{-|e|}{2v_{zo}} \sin(\tfrac{\omega}{c} y_{go}) \int_{z_{in}}^{z} dz' E(z') \cos \theta^{(0)} \tag{12c}$$

$$\theta^{(1)} = \frac{|e|}{2v_{zo}} \frac{v_{\perp o}\omega}{p_{zo}c^2} \sin(\tfrac{\omega}{c} y_{go}) \int_{z_{in}}^{z} dz' \int_{z_{in}}^{z'} dz'' E(z'') \cos \theta^{(0)}(z'') + \frac{1}{p_{\perp o}} \frac{\partial p_{\perp}^{(1)}}{\partial \theta_o}, \tag{12d}$$

where $\Delta\omega = \omega - \Omega_o/\gamma_o$ is the frequency mismatch.

Now substituting (12) into (11) and carrying out the y_{go} integration we arrive at the following expression for the linear efficiency

$$\eta = \frac{-(|e|/m_o c^2)^2}{8\beta_{zo}^2 \gamma_o (\gamma_o - 1)} \int_{z_{in}}^{z_{out}} dz \int_{z_{in}}^{z} dz' \left\{ E(z) E(z') \cos(\tfrac{\omega}{c} (z'-z) \frac{\Delta\omega/\omega}{\beta_{zo}}) + \right.$$

$$\left. \frac{\omega/c}{2\beta_{zo}} \beta_{\perp o}^2 \int_{z_{in}}^{z'} dz'' E(z) E(z'') \sin(\tfrac{\omega}{c} (z''-z) \frac{\Delta\omega/\omega}{\beta_{zo}}) \right\}, \tag{13}$$

where E(z) denotes the profile of the radiation beam. In the present case the radiation beam has a Gaussian profile given by $E(z)=E_o \exp(-z^2/r_o^2)$. Substituting this form for E(z) into (13) and taking the beam entrance and exit planes to be respectively $z_{in}=-\infty$ and $z_{out}=\infty$, the integrations over z, z' and z'' can be carried out analytically. The overall expression for the linear, small signal, efficiency takes the rather simple form

$$\eta = \frac{\pi}{16} \frac{\gamma_o}{\gamma_o - 1} \left(\frac{E_o}{B_o}\right)^2 \xi_o^2 \, e^{-\frac{1}{2}(\xi_o \Delta\omega/\omega)^2} \left[\frac{\beta_{\perp o}^2}{2} \xi_o^2 \frac{\Delta\omega}{\omega} - 1\right], \tag{14}$$

where $\xi_o = (r_o\omega/c)/\beta_{zo}$. Unlike the case of a beam propagating along the z axis, the structure of η is non-oscillating in, say, r_o. The reason for this is that the radiation field is a smooth function of z and has no

abrupt change in behavior at the entry and exit points of the electrons. From (14) we see that the efficiency is positive when $\Delta\omega/\omega > 2/(\beta_{\perp 0}\xi_0)^2$, hence, the output frequency is always slightly higher than the relativistic cyclotron frequency. For typical choices of parameters, the term $\beta_{\perp 0}^2\xi_0^2(\Delta\omega/\omega)/2$ is much greater than unity. In this case the linear efficiency maximizes when the frequency shift is $\Delta\omega = \omega/\xi_0$.

Appendix A contains a derivation of the small-signal efficiency at the fundamental as well as at all cyclotron harmonics using the linearized Vlasov equation. In this appendix the linear efficiency expression is derived for the cases where the electric field of the radiation beam is polarized in the x direction, i.e., polarization considered in the body of this paper, as well as in the z direction. The former polarization of the electric field is shown to result in substantially higher linear efficiencies compared to the latter polarization. In conventional electron cyclotron masers the particle interacts with the TE mode of the structure. This corresponds, in our present configuration, to the electric field polarized in the x direction. Polarization of the electric field in the z direction would correspond to a TM mode interaction in the conventional configuration.

In order for the system to operate in the assumed steady state, there must be losses which just compensate for the power loss of the electron beam. These losses are composed of both the output radiated power, and the real losses due to diffraction or dissipation in the mirrors. All of these losses are characterized by the Q of the cavity so that the total power out of the resonator is $P_{out} = \omega \mathcal{E}_{stored}/Q$, where

$\mathcal{E}_{stored}$ is the energy stored in the cavity, which is proportional to E_o^2. Since linear theory shows that power lost by the beam is also proportional to E_o^2, the operating field amplitude cannot be determined by linear theory alone. Thus the oscillator, unlike the amplifier, is an inherently nonlinear device.

As will be shown in the next section, where the nonlinear electron dynamics are calculated, the power lost by the beam ultimately levels off as E_o^2 increases. Thus the actual operating point can be calculated from the intersection of the graphs of power loss by the beam, and power lost by the cavity, as functions of E_o^2, shown schematically in Figure 3. It is apparent that steady state can be achieved only if the losses are small enough that the two curves intersect. Also, for the optical cavity configuration, we find that the power lost by the beam never becomes negative as E_o^2 increases. Thus steady state operation is not possible without power loss by the cavity.

The threshold condition for starting the oscillations in the resonator is

$$\eta\, P_{b,in} \geq \omega \mathcal{E}_{stored}/Q \ , \tag{15}$$

where $\mathcal{E}_{stored} = \frac{1}{4}(E_o^2/8\pi)\, \pi r_o^2 L$ is the stored field energy. To obtain the threshold electron beam power, necessary to start the resonator, we use the small-signal efficiency in Eq. (14). Substituting the maximum small-signal efficiency, i.e., when $\xi_o \Delta\omega/\omega = 1$, into (15) we find that the product of the beam power and resonator Q needed to start the oscillations is

$$P_{b,in} Q \geq 4.6 \times 10^9 \ \frac{L}{r_o}\ \gamma_o(\gamma_o - 1)\beta_{zo}^3/\beta_{\perp o}^2 \text{[watts]} \ . \tag{16}$$

Throughout our analysis on the quasi-optical maser we have made the tacit assumption that the energy lost by the electrons goes into supporting the assumed Gaussian radiation beam. This assumption is common to all conventional oscillator problems and has been proven valid experimentally. Though we have not rigorously proven this point, concerning our present configuration, we have assumed it applies here too.

III. NUMERICAL RESULTS AND ILLUSTRATIONS

a) Efficiency of Maser in Uniform External Magnetic Field

As an illustration of the potential operation of the quasi-optical maser we choose a 60 keV (γ_o = 1.118) electron beam having initial velocity components $\beta_{\perp o}$= 0.4 and β_{zo}= 0.2. The location and curvature of the mirrors are chosen so that the radiation spot size is 5.9 wavelengths, i.e. r_o= 5.9λ. The linear (small signal) efficiency given by (14) is shown in Figure (4) for various values of the normalized field amplitude, E_o/B_o. The linear efficiency has a single positive maximum when $\xi_o\Delta\omega/\omega$ = 1 which corresponds to the frequency $\omega_{max}=(1-1/\xi_o)^{-1}\Omega_o/\gamma_o$. The intermode frequency separation of a resonator of length L is $\delta\omega = \pi c/L$. Therefore, a spectrum of natural modes can exist within the resonator separated in frequency by $\delta\omega$. When the oscillator is first started up, the mode frequency closest to ω_{max} will be excited first and grow to a level where it suppresses the slower growing natural modes further away from ω_{max}. It turns out that the maximum non-linear efficiency occurs at a frequency slightly higher than ω_{max}, i.e., for $\xi_o\Delta\omega/\omega$ somewhat larger than unity.

In the absence of longitudinal mode selection or equivalent scheme,it would not be possible to take advantage of the higher non-linear efficiencies occurring at frequencies greater than ω_{max}. To suppress these unwanted modes near ω_{max} and operate the maser at the frequency of maximum non-linear efficiency, we will assume that a longitudinal mode selector[26] is employed. Another approach seems possible: we can start the oscillator at the natural operating frequency ω_{max}. When the mode saturates, the external magnetic field can be decreased

slightly so that $\xi_0 \Delta\omega/\omega \gtrsim 1$ has the appropriate value to maximize the non-linear efficiency. We will assume that, by using either of these approaches, the operating frequency can be freely chosen.

The non-linear efficiency defined in Eq. (11), is evaluated by following numerically the particle trajectories according to (6). For sufficiently small field amplitudes, the simulations reproduced very accurately the linear efficiency in (13). The beam entry and exit points were taken at $\pm 2r_0$ and the electron orbits were integrated using a 4-point Runge-Kutta integrator. Figure (5) demonstrates the higher non-linear efficiencies achievable at larger values of $\xi_0 \Delta\omega/\omega$. The efficiency in this figure is obtained by solving (11) as a function of E_0/B_0 for various values $\xi_0 \Delta\omega/\omega$. A maximum efficiency of 33% is obtained for $\xi_0 \Delta\omega/\omega = 7$ at $E_0/B_0 = 2.25 \times 10^{-2}$. Figures (6) and (7) show the spatial variation of the efficiency within the resonator for various values of the normalized frequency shift $\xi_0 \Delta\omega/\omega$ and normalized field amplitude E_0/B_0. The spatial oscillations in efficiency within the resonator are due to the oscillations of the trapped particle distribution. The Gaussian profile of the radiation beam is also shown in Figure (5) for reference purposes.

The examples presented so far should not lead to the impression that good performance is necessarily associated with frequency mismatches significantly larger than the values corresponding to maximum linear gain. For example, for a beam with $\beta_{\parallel 0} = 0.1$ and $\beta_{\perp 0} = 0.2$, corresponding to $\gamma_0 = 1.026$ (13.3 keV), the nonlinear efficiency is plotted in Fig. 8 against the radiation field amplitude for various values of the ratio r_0/λ. In all cases the frequency mismatch was taken to correspond to the maximum linear

gain value, obtained from Eq. (14). As can be seen in Fig. 8, a peak efficiency of 20% is obtained for $r_o/\lambda = 2.5$, while the values of $\eta = 17.5\%$ are obtained for $r_o/\lambda = 1.6$ and 3.2. For these cases, the frequency mismatch is given by $\Delta\omega/\omega = 0.75 \times 10^{-2}$, 1.30×10^{-2} and 0.58×10^{-2}, respectively, and corresponds to optimal linear gain value.

b) Efficiency Enhancement By Contouring External Magnetic Field

It is possible to enhance the non-linear operating efficiency of the quasi-optical maser by either pre-bunching the electron beam in momentum phase angle $\omega\tau - \Theta$ or by appropriately contouring the external magnetic field. Pre-bunching the electron beam, by utilizing a two open resonator Klystron type configuration, is in principle straightforward and results in extremely high efficiencies. However, depending on the length of the ballistic phase bunching region (distance between the two resonators), electron beam thermal effects may present a problem at high frequencies. Contouring the magnetic field appears to be the simplest method for enhancing efficiency. By slightly contouring the magnetic field, as a function of z, a more advantageous momentum phase distribution of the electrons can be realized with a single resonator. A significant improvement in efficiency over the already highly efficient uniform magnetic field case can be realized in this way. Figure 9 shows the spatial evolution of efficiency with and without magnetic field contouring. The magnetic field in this case was decreased linearly by 5% between the points $z = -2r_o$ and $z = 2r_o$. For this variation a final total efficiency of 45% was achieved.

c) Design Examples

We conclude with two specific detailed design examples, which will demonstrate the potential of the configuration we have analyzed. In the

following examples the steady state performance of the maser, operating at 150 GHz (λ = 2 mm), is analyzed. The electron beam is taken to be generated by a diode with a current density of 10 A/cm^2. Within the oscillator, the electron beam has a rectangular cross section,[27] with area $A = 2r_o y_R$, extending from $x = -r_o/2$ to $x = +r_o/2$ and from $y = -y_R$ to $y = +y_R$, where r_o is the spot size and y_R is the Rayleigh length.

The first example deals with the 60 keV beam with $\beta_{\perp o} = 0.4$ and $\beta_{\parallel o} = 0.2$, for which the efficiency is shown in Fig. 5. For $r_o/\lambda = 5.9$, the beam cross section is $A = 52$ cm^2, giving a beam current of 520 A and an input beam power of 31 MW. Due to the slight variations of the radiation field amplitude across the beam, the conversion efficiency has to be appropriately averaged. For a radiation field of magnitude $E_o/B_o = 2.4 \times 10^{-2}$ at the center of the beam, this weighted average efficiency is $\eta = 28\%$, hence the radiated output power is $P_{rad} = 8.7$ MW. For such performance, a normalized frequency mismatch $\xi_o \Delta\omega/\omega = 7$ is required, hence $\Delta\omega/\omega = 3.77\%$ and $\omega/\Omega_o = 0.93$. For $\lambda = 2$ mm ($\omega = 9.4 \times 10^{11}$ sec^{-1}), a magnetic field of $B_o = 58$ kG is required. In addition, by appropriately tapering the external magnetic field the output power can be increased to $P_{rad} = 12$ MW. Finally, if either of the above illustrations (with or without the external field taper) is to be achieved by initially adjusting the external magnetic field to the value corresponding to maximum linear gain of the operating frequency, then for a 44 cm long resonator (i.e., equal to 2 y_R), the value of Q obtained from (16) must exceed the 180, while the operating value of Q is 40,000.

In the above example the frequency mismatch was substantially higher than the value required for maximum linear gain. The highly impressive

performance associated with the adaptation of such a condition warrants its implementation. The realization of such a large frequency mismatch would require a mode selector or an external source to set up the radiation field. However, if such complications are to be avoided, excellent performance can be achieved as will be shown. In the second example we consider a 13.3 keV beam with $\beta_{\|o} = 0.1$ and $\beta_{\perp o} = 0.2$, interacting with a radiation beam of $\lambda = 0.2$ cm and $r_o/\lambda = 2.5$, at the frequency mismatch associated with maximum linear gain, i.e. $\Delta\omega/\omega = 0.75\%$. In this case, the cross-sectional area of the beam is $A \simeq 4\ cm^2$. Assuming that the diode current density of 10 A/cm^2 can be compressed to 50 A/cm^2, the input beam power is 2.7 MW. For $E_o/B_o = 2.3 \times 10^{-3}$, the average efficiency is 18%, hence the radiation power is $P_{rad} = 0.50$ MW. The required value of the external magnetic field is $B_o = 54.5$ kG. For this case, the linear threshold condition (16) is not restrictive, since it simply requires that the nonlinear efficiency be smaller than the linear value, which is the case. Assuming an oscillator length equal to 16 $y_R = 63$ cm, the operating value Q is 1560, larger than the threshold value of 150, required by (16).

REFERENCES

1. J. M. J. Madey, H. A. Schwettman and W. M. Fairbrank, IEEE Trans. Nucl. Sci. 20, 980 (1973).
2. P. Sprangle and V. L. Granatstein, Appl. Phys. Lett. 25, 377 (1974).
3. W. B. Colson, Phys. Lett. A 59, 187 (1976).
4. T. Kwan, J. M. Dawson and A. T. Lin, Phys. Fluids 20, 581 (1977).
5. N. M. Kroll and W. A. McMullin, Phys. Rev. A 17, 300 (1978).
6. A. Gover and A. Yariv, Appl. Phys. 16, 121 (1978).
7. P. Sprangle, Cha-Mei Tang and W. M. Manheimer, Phys. Rev. Lett. 43, 1932 (1979).
8. P. Sprangle and R. A. Smith, Phys. Rev. A 21, 293 (1980).
9. N. M. Kroll, P. Morton and M. N. Rosenbluth, JASON Tech. Report JSR-79-15, 1980.
10. R. Q. Twiss, Australian J. Phys. 11, 564 (1958).
11. A. V. Gaponov, Izv.VUZ Radiofizika, 2, 450 (1959).
12. R. H. Pantell, Proc. IRE, 47, 1146 (1959).
13. M. Borenstein and W. E. Lamb, Jr., Phys. Rev. A 5, 1298 (1972).
14. E. Ott and W. M. Manheimer, IEEE Trans. Plasma Sc., PS-3, 1 (1975).
15. P. Sprangle and W. M. Manheimer, Phys. Fluids 18, 224 (1975).
16. P. Sprangle and A. T. Drobot, IEEE Trans. MTT-25, 528 (1977).
17. K. R. Chu, Phys. Fluids 21, 2354 (1978).
18. P. Sprangle and R. A. Smith, NRL Memo. Report 3983 (1979).
19. K. R. Chu, M. E. Read and A. K. Ganguly, IEEE Trans. MTT-28, 318 (1980).
20. L. R. Elias, W. M. Fairbank, J. M. J. Madey, H. A. Schwettman and T. I. Smith, Phys. Rev. Lett. 36, 717 (1976).

21. D. B. McDermott, T. C. Marshall, S. P. Schlesinger, R. K. Parker and V. L. Granatstein, Phys. Rev. Lett. 41, 1368 (1978).

22. J. L. Hirshfield and J. M. Wachtel, Phys. Rev. Lett. 12, 533 (1964).

23. A. A. Andronov, V. A. Flyagin, A. V. Gaponov, A. L. Gol'denberg, M. I. Petelin, V. G. Usov and V. K. Yulpatov, Infrared Phys. 18, 385 (1978).

24. J. L. Seftor, V. L. Granatstein, K. R. Chu, P. Sprangle and M. E. Read, IEEE J. Quantum Electronics, QE-15, 848 (1979).

25. M. E. Read, R. M. Gilgenbach, R. Lucey, Jr., K. R. Chu, A. T. Drobot and V. L. Granatstein, IEEE Trans., MTT, in press (1980).

26. P. W. Smith, IEEE J. Quantum Electronics, QE-1, 343 (1965).

27. The introduction of a rectangular beam relaxes the perveance requirements by approximately r_o/Y_R .

APPENDIX A

Here we work out the steady state linear theory for the energy loss of the electron beam as it traverses the wave fields in the open resonator. In steady state, the energy equation for the beam is

$$\frac{\partial}{\partial z} W_{f\ell} = \underset{\sim}{E} \cdot \underset{\sim}{J} \ , \tag{A1}$$

where $W_{f\ell}$ is the beam energy flux and $\underset{\sim}{J}$ is the beam current. The configuration is as shown in Figure 1. The change in beam power as it crosses the resonator then is $\int d^3r \ \underset{\sim}{E} \cdot \underset{\sim}{J}$, so the main problem is to calculate an expression for the perturbed beam current density $\underset{\sim}{J}$.

This can most easily be done by analyzing the linearized Vlasov equation

$$\left(-i\omega + \underset{\sim}{v} \cdot \underset{\sim}{\nabla} - \frac{|e| \underset{\sim}{p} \times \underset{\sim}{B}_o}{\gamma m_o c} \cdot \frac{\partial}{\partial \underset{\sim}{p}}\right) f^{(1)} = |e| \left(\delta \underset{\sim}{E} + \frac{\underset{\sim}{p} \times \delta \underset{\sim}{B}}{\gamma m_o c}\right) \cdot \frac{\partial f^{(0)}}{\partial \underset{\sim}{p}} , \tag{A2}$$

where a time dependence $e^{-i\omega t}$ is assumed. The quantity $f^{(0)}$ is the unperturbed distribution function, that is, the distribution function at $z=-\infty$, and $f^{(1)}$ is the perturbation to it induced by the fields in the resonator. Instead of using independent variables $\underset{\sim}{r}$, $\underset{\sim}{p}$, it is more convenient to use as independent variables the quantities $(x_g, y_g, z, p_\perp, \phi, p_z)$ where

$$p_x = p_\perp \cos\left(\frac{\Omega_o m_o}{p_z} z + \phi\right)$$

$$p_y = p_\perp \sin\left(\frac{\Omega_o m_o}{p_z} z + \phi\right) , \tag{A3}$$

and

$$x = x_g + \frac{p_\perp \sin\left(\frac{\Omega_o m_o}{p_z} z + \phi\right)}{m_o \Omega_o} \tag{A4}$$

$$y = y_g - \frac{p_\perp \cos\left(\frac{\Omega_o m_o}{p_z} z + \phi\right)}{m_o \Omega_o} ,$$

where Ω_0 is the nonrelativistic cyclotron frequency. These have the advantage of being constant in the absence of the radiation fields in the resonator. In these new variables, the Vlasov equation reduces to

$$\left(-i\omega + \frac{p_z}{\gamma m_0} \frac{\partial}{\partial z}\right) f^{(1)} = |e|\left(\delta\underset{\sim}{E} + \frac{\underset{\sim}{p} \times \delta\underset{\sim}{B}}{\gamma m_0 c}\right) \cdot \frac{\partial f^{(0)}}{\partial \underset{\sim}{p}} , \tag{A5}$$

and assuming that $f^{(0)}$ is independent of ϕ, $\frac{\partial f^{(0)}}{\partial \underset{\sim}{p}}$ reduces to

$$\frac{\partial f^{(0)}}{\partial p} = \left\{ \hat{e}_x \left(2p_\perp \cos\left(\frac{\Omega_0 m_0}{p_z} z + \phi\right) \frac{\partial}{\partial p_\perp^2} + \frac{1}{\Omega_0 m_0} \frac{\partial}{\partial y_g}\right) + \hat{e}_y \left(2p_\perp \sin\left(\frac{\Omega_0 m_0}{p_z} z + \phi\right)\right.\right.$$

$$\left.\left. \frac{\partial}{\partial p_\perp^2} - \frac{1}{\Omega_0 m_0} \frac{\partial}{\partial x_g}\right) + \hat{e}_z \frac{\partial}{\partial p_z} \right\} f^{(0)} . \tag{A6}$$

There are two possible polarizations for the radiation. The first is

$$\delta\underset{\sim}{E} = E(z) \cos ky \, e^{-i\omega t} \hat{e}_x + \text{c.c.}$$

$$\delta\underset{\sim}{B} = \frac{ikc}{\omega} E(z) \sin ky \, e^{-i\omega t} \hat{e}_z + \text{c.c.} , \tag{A7}$$

which we call TE since it has $\delta\underset{\sim}{E} \perp \underset{\sim}{B}_0$. The second polarization

$$\delta\underset{\sim}{E} = E(z) \cos ky \, e^{-i\omega t} \hat{e}_z + \text{c.c.}$$

$$\delta\underset{\sim}{B} = \frac{-ikc}{\omega} E(z) \sin ky \, e^{-i\omega t} \hat{e}_x + \text{c.c.} , \tag{A8}$$

is TM since $\delta\underline{B} \perp \underline{B}_0$.

For TE polarization, the linearized Vlasov equation reduces to

$$\left(\frac{\partial}{\partial z} - \frac{i\gamma m_0 \omega}{p_z}\right) f^{(1)} = \frac{\gamma m_0}{p_z} \frac{|e|E(z)}{2\omega} e^{i(ky-\omega t)} \left\{ 2\omega p_\perp \cos\left(\frac{\Omega_0 m_0 z}{p_z} + \phi\right) \frac{\partial}{\partial p_\perp^2} \right.$$

$$\left. + \left(\omega - \frac{kp_\perp}{\gamma m_0} \sin\left(\frac{\Omega_0 m_0 z}{p_z} + \phi\right)\right) \frac{1}{\Omega_0 m_0} \frac{\partial}{\partial y_g} - \frac{kp_\perp}{\gamma m_0} \frac{1}{\Omega_0 m_0} \cos\left(\frac{\Omega_0 m_0 z}{p_z} + \phi\right) \frac{\partial}{\partial x_g} \right\} f^{(0)}$$

$$+ (k \to -k) \equiv G(z) . \tag{A9}$$

The perturbed distribution function then is

$$f^{(1)} = \exp\left(i\frac{\gamma m_o \omega z}{p_z}\right)\int_{-\infty}^{z} dz' \exp\frac{-i\gamma m_o \omega z'}{p_z} G(z'), \qquad \text{(A10)}$$

The quantity we are interested in is $\int_{\Omega_o m_o z} \delta E^* \cdot \delta J \, d^3r$ which is

$$-|e|\int p_\perp dp_\perp dp_z d\phi dx_g dy_g dz \;\; (p_\perp/\gamma m_o)\cos\left(\frac{\Omega_o m_o z}{p_z} + \phi\right) \;\; \delta E^* f^{(1)} .$$

In doing this integral, exp(iky), which appears in the expression for δE must be written as $\exp\{ ik [y_g - (p_\perp/\Omega_o m_o) \cos (\Omega_o m_o z/p_z + \phi)]\}$ which is equal to

$$\sum_n J_n\left(\frac{kp_\perp}{\Omega_o m_o}\right) \exp i\left(ky_g + ni\left[\frac{\pi}{2} \;\; \frac{\Omega_o m_o z}{p_z} + \phi\right]\right).$$

Then $\int E^* \cdot J \, d^3r$ is given by

$$\int d^3r \; E^* \cdot J = \frac{1}{4}\int dx_g dy_g dz \; p_\perp dp_\perp d\phi dp_z \;\; E^*(z)\sum_{n'=-\infty}^{\infty} J_{n'}\left(\frac{kp_\perp}{\Omega_o m_o}\right)\exp\left[-in'\left(\frac{\Omega_o m_o z}{p_z} + \phi - \frac{\pi}{2}\right)\right]$$

$$\int_{-\infty}^{z} dz' \exp\left[i\frac{\gamma m\omega(z-z')}{p_z}\right]\left(\frac{-|e|^2}{\omega}\right) E(z)\sum_{n=-\infty}^{\infty} J_n\left(\frac{kp_\perp}{\Omega_o m_o}\right)\exp\left[i\, n\left(\frac{\Omega_o m_o z}{p_z} + \phi - \frac{\pi}{2}\right)\right]$$

$$\frac{p_\perp}{p_z}\cos\left(\frac{\Omega_o m_o z}{p_z} + \phi\right)\cos\left(\frac{\Omega_o m_o z}{p_z} + \phi\right)\left(2\omega p_\perp \frac{\partial f^{(0)}}{\partial p_\perp^2}\right) + (k \to -k) + \text{c.c.} , \qquad \text{(A11)}$$

where we have assumed that $\frac{\partial f^{(0)}}{\partial y_g} = 0$, that is, the distribution of guiding centers is uniform in the y direction (actually the dimension of the beam in the y direction is very long compared to a wavelength), and also have exploited the fact that no quantity except $f^{(0)}$ depends on x_g, so the $\frac{\partial f^{(0)}}{\partial x_g}$ term integrates to zero. Since $f^{(0)}$ is independent of ϕ, the

only term which does not integrate to zero over ϕ is the zero Fourier harmonic. This collapses the double summation over n and n′ into a single summation, so that

$$\int d^3r\ \underset{\sim}{E}^*\cdot\underset{\sim}{J}=2\pi|e|^2\int dx_g dy_g dz\ p_\perp dp_\perp dp_z\ E^*(z)\sum_{n=-\infty}^{\infty}\left[J_n'\left(\frac{kp_\perp}{m_o\Omega_o}\right)\right]^2$$

$$\int_{-\infty}^{z}dz'\exp\left\{i\left[\frac{\gamma m_o\omega}{p_z}-\frac{\Omega_o m_o}{p_z}\right](z-z')\right\}\left\{\frac{p_\perp^2}{p_z}\frac{\partial f^{(o)}}{\partial p_\perp^2}+\text{c.c.}\right., \qquad \text{(A12)}$$

where the $(k\rightarrow -k)$ has now been explicitly included.

The next problem is to do the zz′ integral. Assuming E(z) has the form $E_o \exp(-z^2/r_o^2)$, this integral is of the form

$$\int_{-\infty}^{\infty}dz\int_{-\infty}^{z}dz'\ \exp\left\{-\left[\left(\frac{z}{r_o}\right)^2+\left(\frac{z'}{r_o}\right)^2+i\,\alpha(z-z')\right]\right\}\text{where}\ \alpha=\ (\gamma m_o\omega - n\,m_o\Omega_o)/p_z.$$

By completing the square, the z′ integral can be done in terms of error functions so it reduces to a single integral

$$\frac{\sqrt{\pi}}{2}\,r_o^2\,e^{-\frac{\alpha^2r_o^2}{2}}\int_{-\infty}^{\infty}du\ \exp\left[-(u+i\alpha r_o)^2\right]\left[1+\text{erf}\,u\right]\ .$$

Since the error function is an odd function of u, the integral of the term in the square brackets containing the error function is

$$\int_{-\infty}^{\infty} i\,\sin(2\alpha r_o u)e^{-u^2}\,\text{erf}\,u\ ,$$

which is purely imaginary and sums to zero upon adding the complex conjugate. Thus only the unity in the square brackets contributes to the integral and the total result is

$$\frac{\pi}{2}\,r_o^2\,e^{-\frac{\alpha^2r_o^2}{2}}\ .$$

Hence the total result is

$$\int d^3r\ \underset{\sim}{E}^*\cdot\underset{\sim}{J}\Big|_{TE} = -|e|^2\frac{\pi^2}{2}\int dx_g dy_g dp_\perp^2 dp_z \sum_{n=-\infty}^{\infty} E_o^2\ r_o^2\ \exp\left\{-\left[\left(\frac{\gamma m_o\omega - nm_o\Omega_o}{p_z}\right)^2\ \frac{r^2}{2^o}\right]\right\}$$

$$\left[J_n'\left(\frac{kp_\perp}{\Omega_o m_o}\right)\right]^2 \frac{p_\perp^2}{p_z}\ \frac{\partial f^{(o)}}{\partial p_\perp^2}\ . \qquad \text{(A13)}$$

This is the final result for the power loss of the beam as it traverses the fields in the open resonator. To progress further, assume the distribution function

$$f^{(o)} = \frac{\sigma}{2\pi}\,\delta(p_\perp^2 - p_{\perp o}^2)\,\delta(p_z - p_{zo})\,\delta(x_g)\,, \qquad \text{(A14)}$$

where σ is the surface charge density of the sheet beam. The incident power is

$$W_{f\ell} = L\sigma(\gamma-1)\ \frac{p_z c^2}{\gamma}\ . \qquad \text{(A15)}$$

Assuming n=1, $\omega \simeq \Omega_o/\gamma$, and $J_1'(x) \simeq x/2$ (i.e., $kp_\perp \ll \Omega_o m_o$) the integrals can easily be done and Eq. (14) can be recovered for the efficiency. For n=2 one can also show that the efficiency has the same basic form as Eq. (14), but it is multiplied by an overall factor of

$$\frac{1}{4}\ \frac{k^2 p_\perp^2}{m_o^2\ \Omega_o^2}\ ,$$

which is much less than unity. Thus an interaction at the second harmonic exists, but it is weaker.

For the TM mode an analogous calculation gives the result

$$\int d^3r\ \underset{\sim}{E}^*\cdot\underset{\sim}{J}\Big|_{TM} = -|e|^2\frac{\pi^2}{2}\int dx_g dy_g dp_\perp^2 dp_z \sum_{n=-\infty}^{\infty} r_o^2\ \exp\left\{-\frac{r_o^2}{2}\left[\frac{\gamma\ m_o\omega - nm_o\Omega_o}{p_z}\right]\right\}$$

$$E_o^2\ J_n^2\left(\frac{kp_\perp}{\Omega_o m_o}\right)\left\{\frac{1}{2}\left(1 - \frac{n\Omega_o}{\gamma\omega}\right)\frac{\partial}{\partial p_z} + \frac{n\Omega_o}{\gamma m_o}\ p_z\ \frac{\partial}{\partial p_\perp^2}\right\}\ g\ . \qquad \text{(A16)}$$

At each harmonic, the power loss of the beam is smaller by a factor of order $\left(\frac{kp_\perp}{\Omega_o m_o}\right)^2$ from what it was for the same harmonic with TE polarization. Thus the coupling of the TM mode with the radiation in the optical cavity is much weaker than for the TE mode.

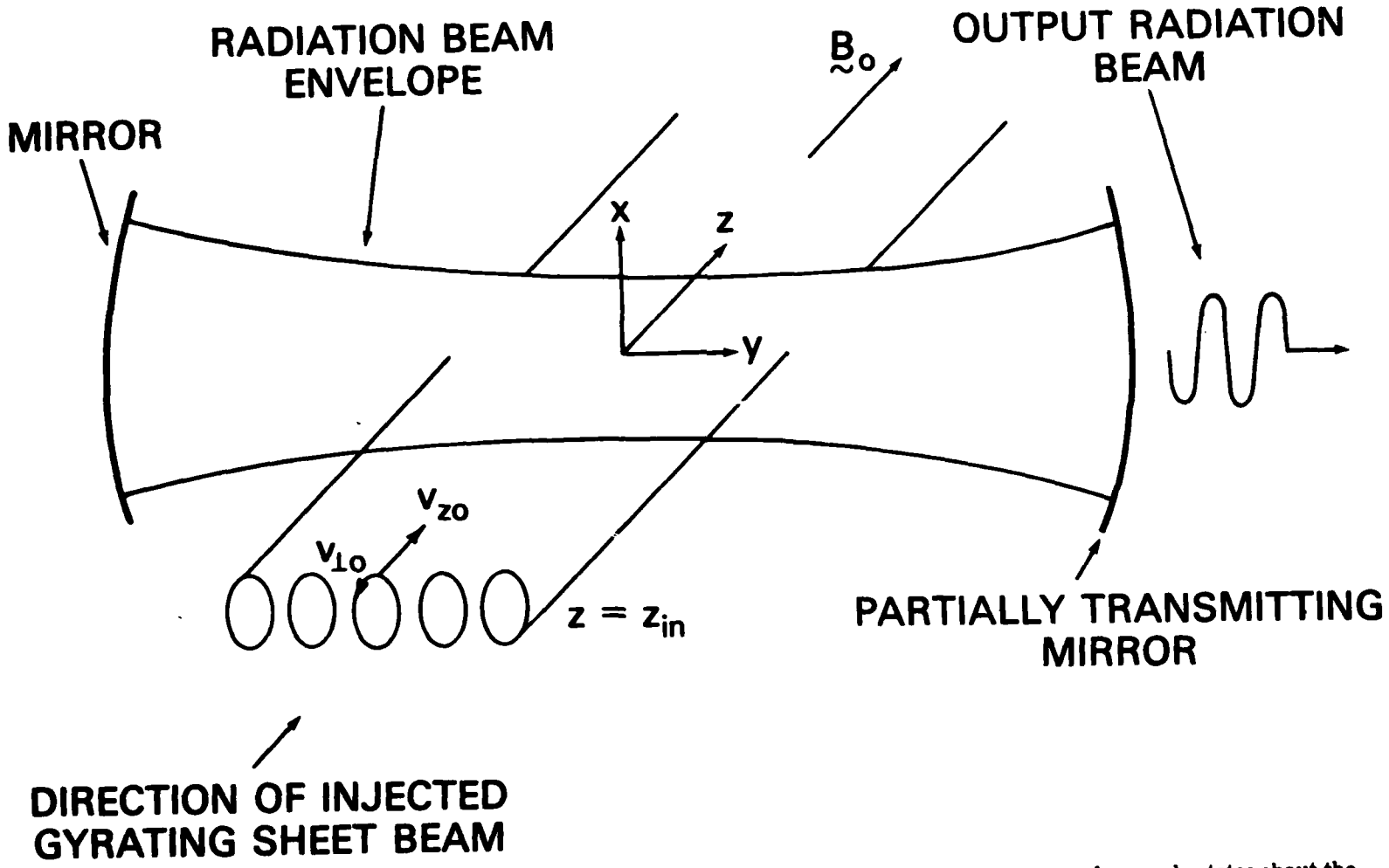

Fig. 1 — Schematic representation of the quasi-optical cyclotron maser. The electron beam propagates along and rotates about the z axis and the radiation beam axis coincides with the y axis.

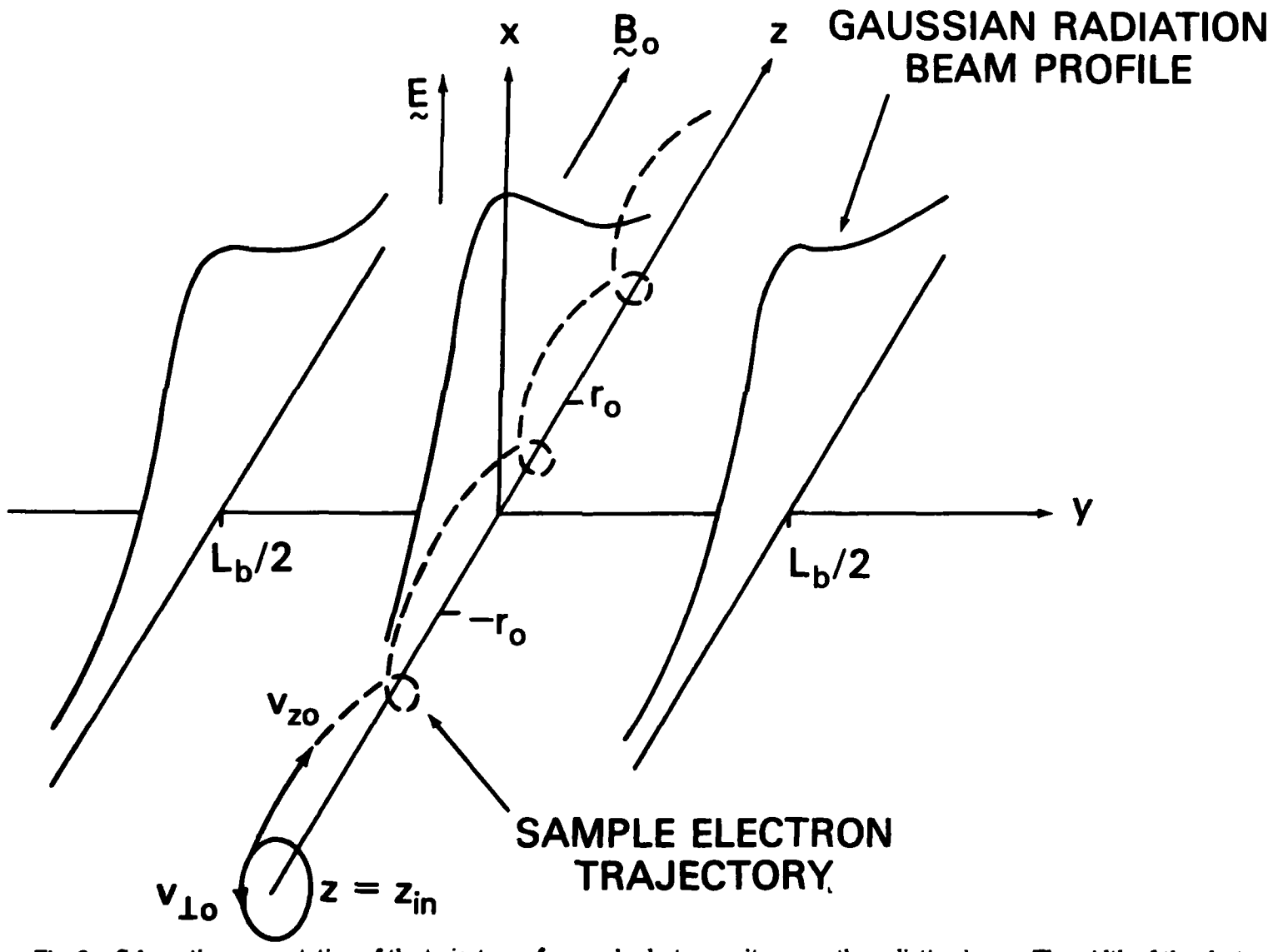

Fig. 2 — Schematic representation of the trajectory of a sample electron as it crosses the radiation beam. The width of the electron beam is L_b.

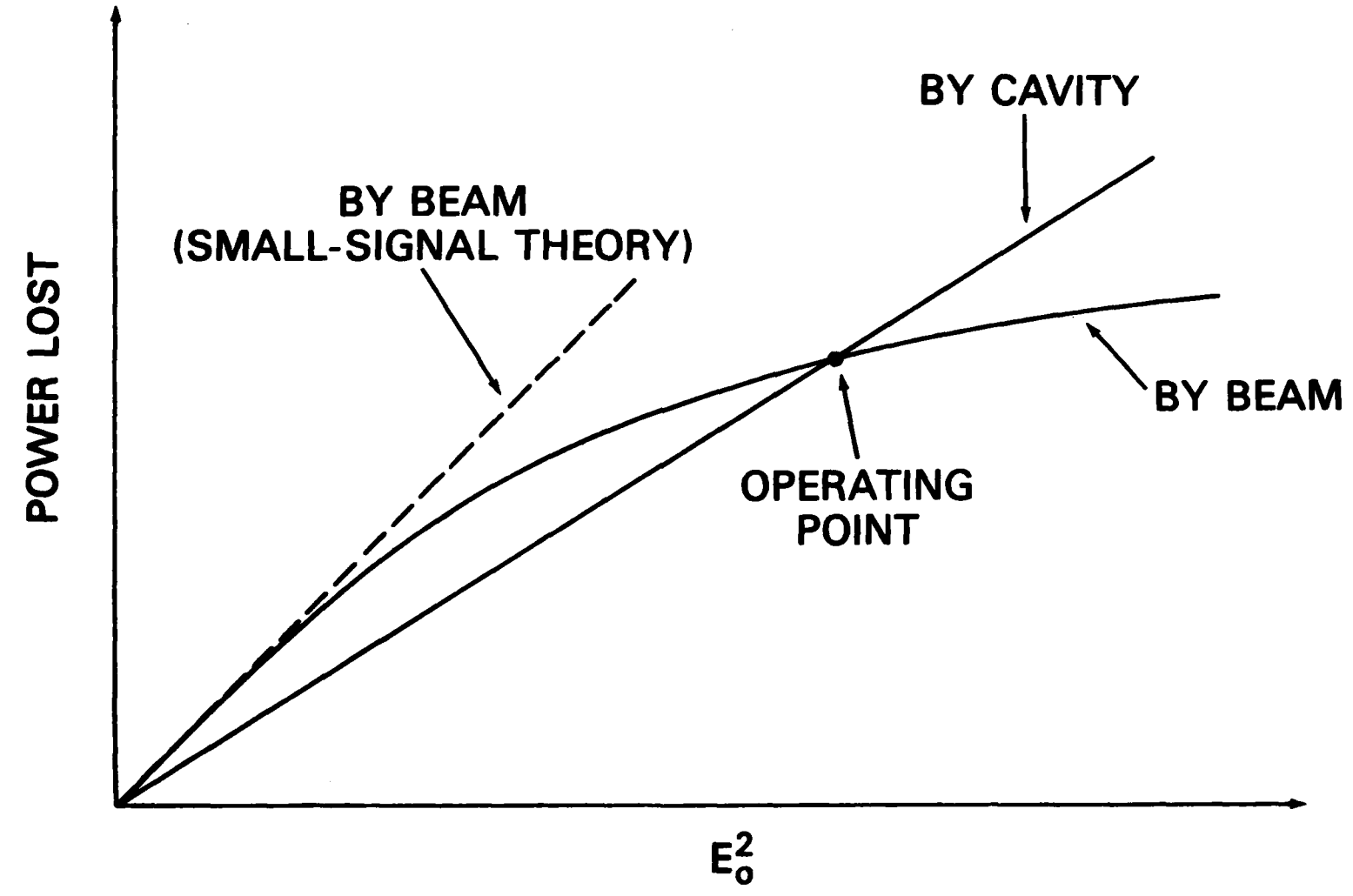

Fig. 3 — Determination of the point of nonlinear steady state operation.

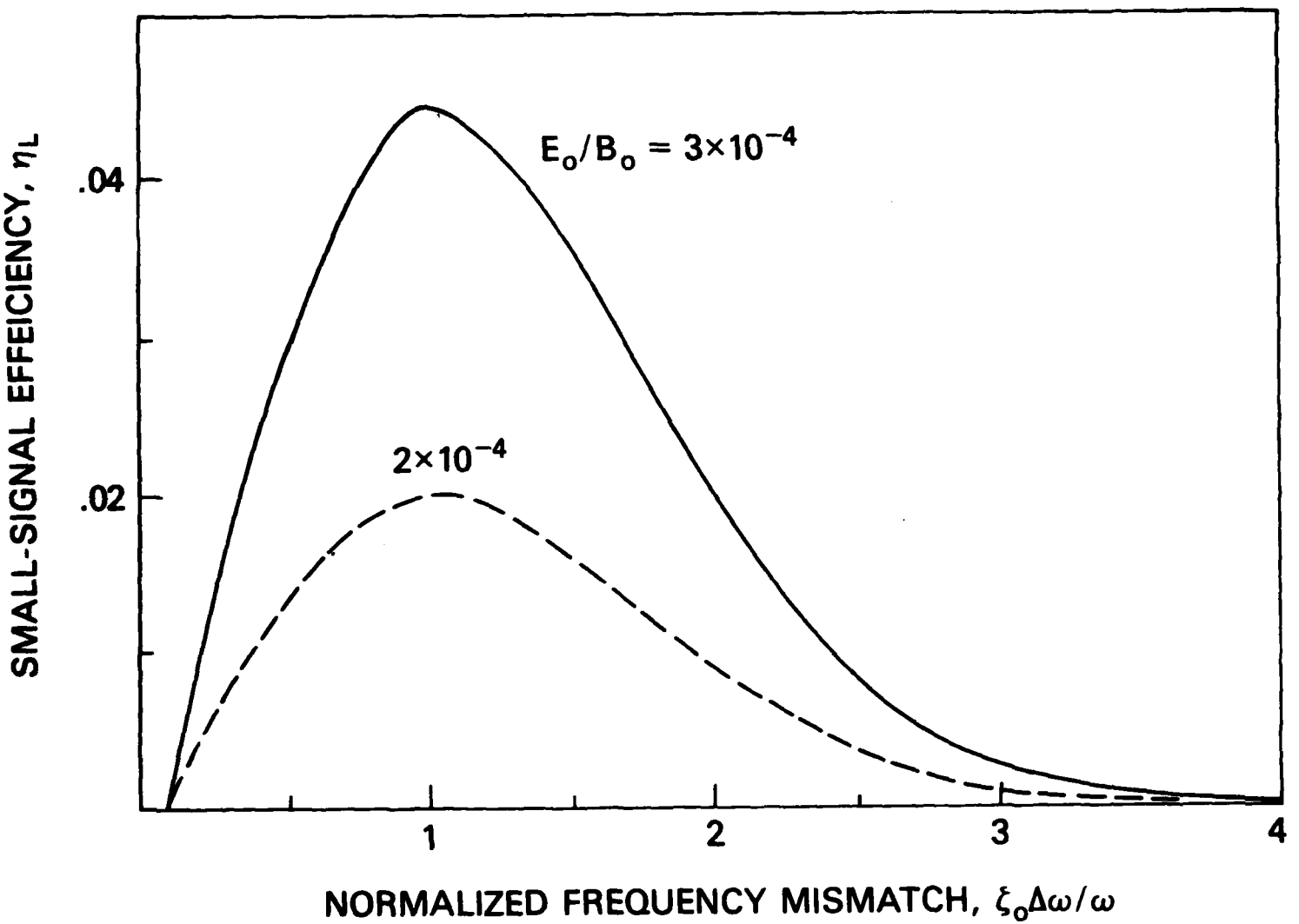

Fig. 4 — Linear efficiency η_L vs. normalized frequency mismatch $\xi_o\Delta\omega/\omega$ for $\beta_{\perp o} = 0.4$, $\beta_{zo} = 0.2$ and $r_o/\lambda = 5.9$.

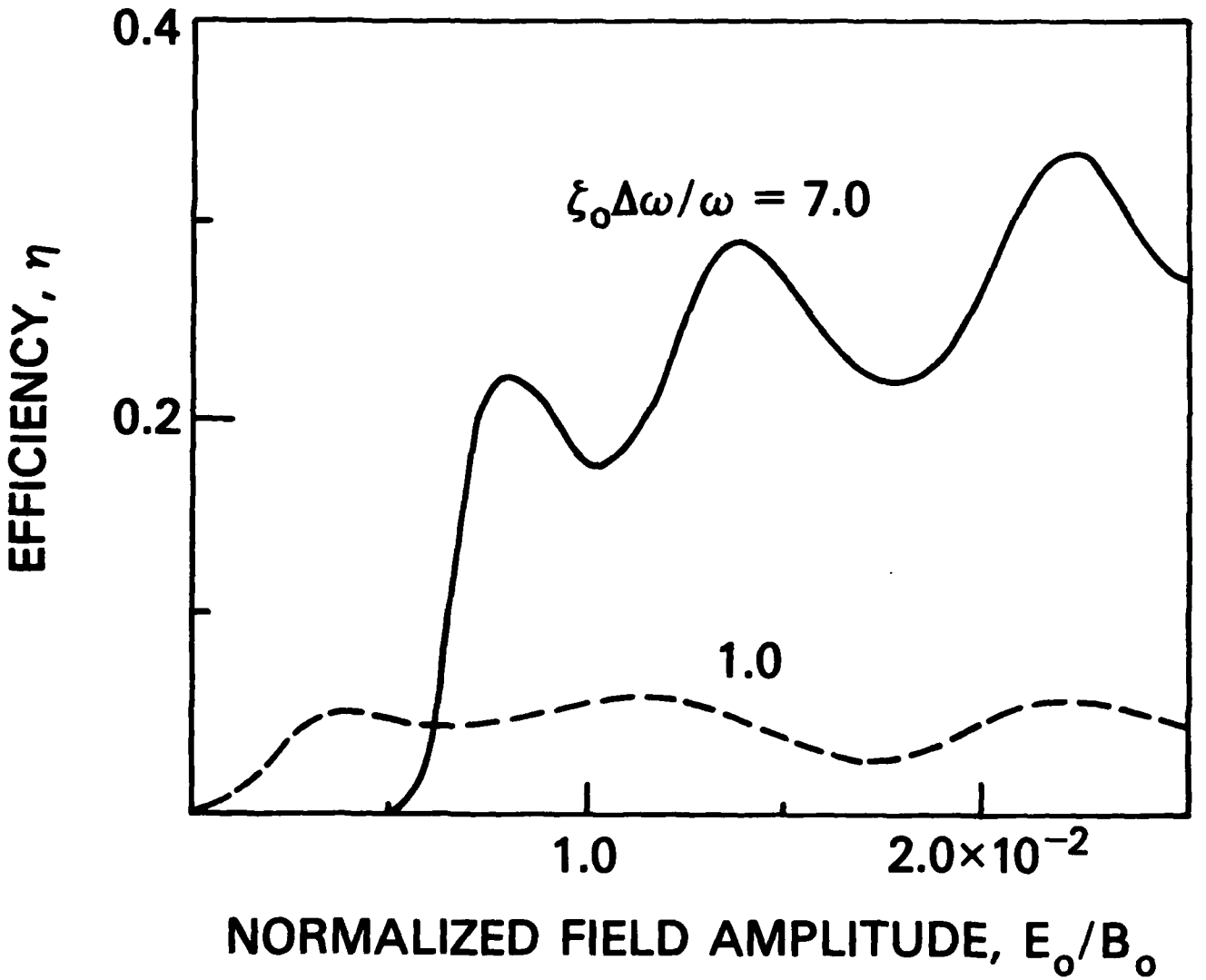

Fig. 5 — Nonlinear efficiency η vs. normalized field amplitude E_o/B_o at the frequency mismatch of optimal (a) nonlinear operation, $\xi_o\Delta\omega/\omega = 7.0$ (solid line) and (b) linear operation, $\xi_o\Delta\omega/\omega = 1.0$ (dashed line). The other parameters are the same as in Fig. 4.

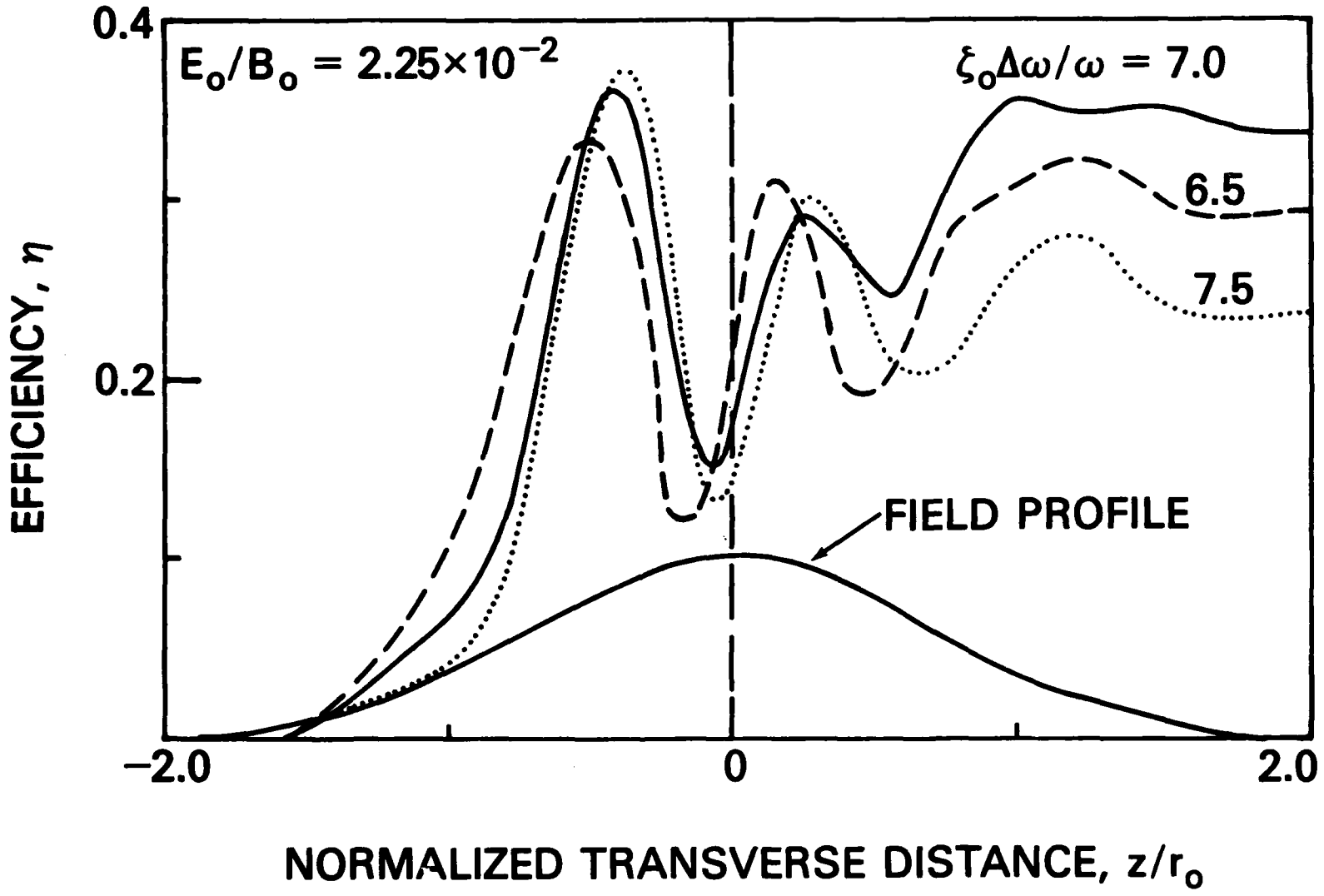

Fig. 6 — Spatial variation of the nonlinear efficiency η across the resonator for the parameters for Fig. 4 at the optimal nonlinear point, $E_o/B_o = 2.25 \times 10^{-2}$ and $\xi_o\Delta\omega/\omega = 7.0$ (solid line), as well at for $\xi_o\Delta\omega/\omega = 6.5$ (dashed line) and $\xi_o\Delta\omega/\omega = 7.5$ (dotted line). The radiation field profile is shown for reference on an arbitrary scale.

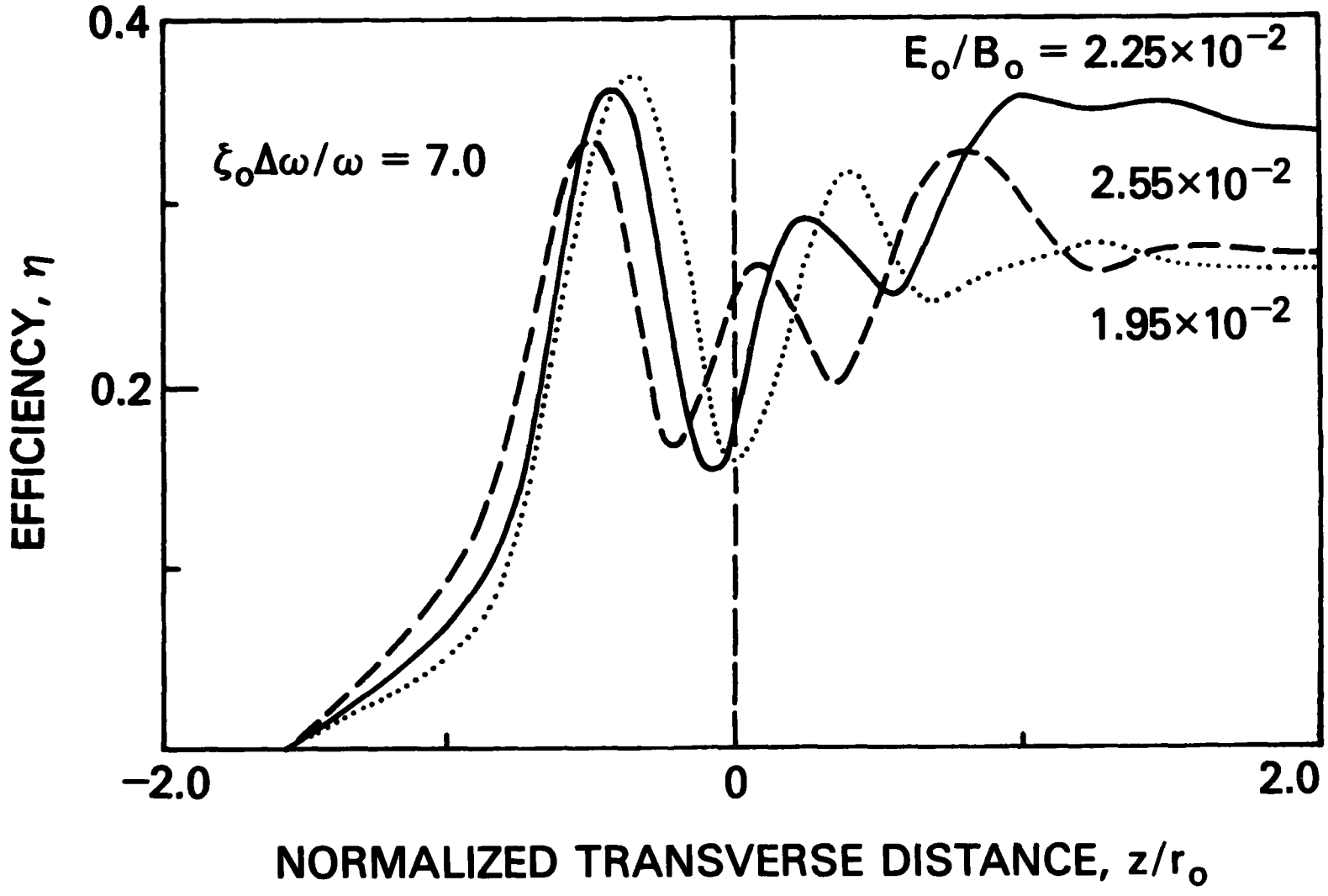

Fig. 7 — Spatial variation of the nonlinear efficiency η across the oscillator for the parameters for Fig. 4 at the optimal nonlinear point, $\xi_o\Delta\omega/\omega = 7.0$ and $E_o/B_o = 2.25 \times 10^{-2}$(solid line), as well as for $E_o/B_o = 2.55 \times 10^{-2}$ (dashed line) and $E_o/B_o = 1.95 \times 10^{-2}$ (dotted line).

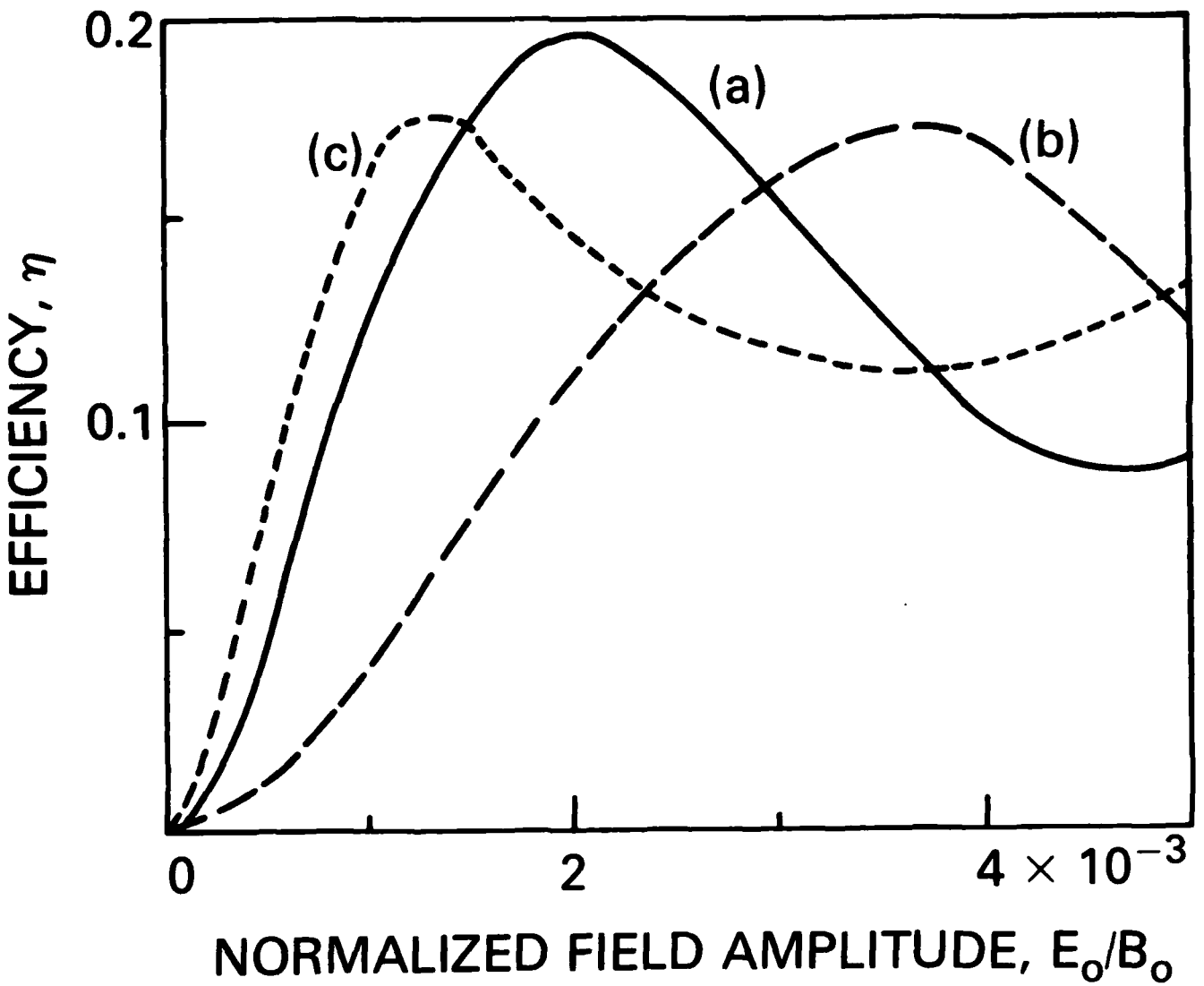

Fig. 8 — Nonlinear efficiency η vs. normalized field amplitude E_o/B_o for $\beta_{\perp o} = 0.2$ and $\beta_{zo} = 0.1$ for operation, when (a) $r_o/\lambda = 2.5$, $\Delta\omega/\omega = 0.75\%$ (solid line), (b) $r_o/\lambda = 1.6$, $\Delta\omega/\omega = 1.30\%$ (dashed line), and (c) $r_o/\lambda = 3.2$, $\Delta\omega/\omega = 0.58\%$ (dotted line).

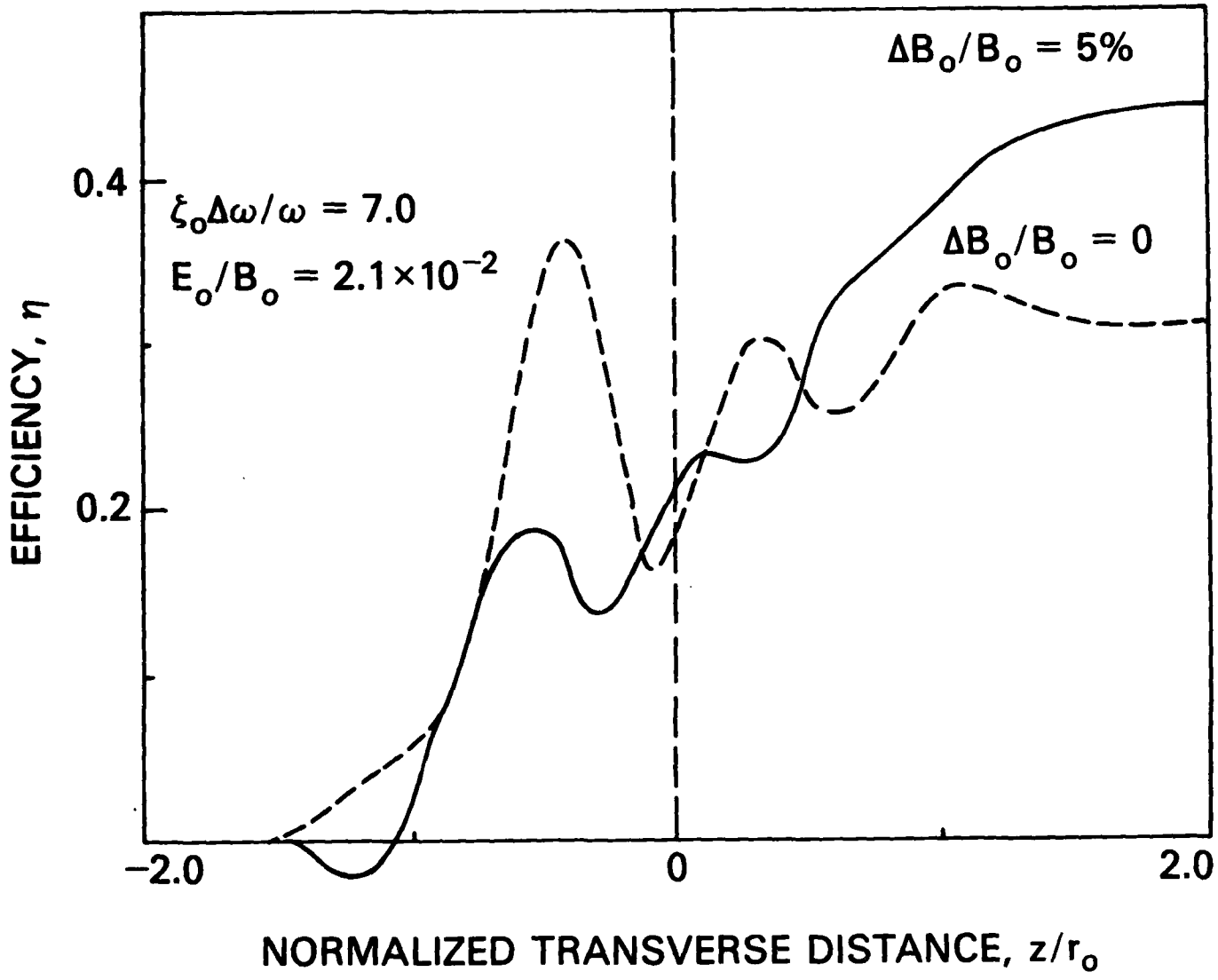

Fig. 9 — Spatial evolution of the nonlinear efficiency η across the oscillator for the parameters of Fig. 4 and for $\xi_o \Delta\omega/\omega = 7.0$ and $E_o/B_o = 2.1 \times 10^{-2}$, (a) when the external magnetic field is decreased by 5% over the distance $4r_o$ (solid line) and (b) when the external magnetic field is uniform (dashed line).

DISTRIBUTION LIST*

Naval Research Laboratory
4555 Overlook Avenue, S.W.
Washington, D.C. 20375

Attn: Code 1000 - CAPT E. E. Henifin
1001 - Dr. A. Berman
4700 - Dr. T. Coffey (25 copies)
4701 - Mr. J. Brown
4740 - Dr. V. L. Granatstein (20 copies)
4740 - Dr. K. R. Chu
4740 - Dr. C. W. Roberson
4740 - Dr. M. E. Read
4790 - Dr. P. Sprangle (100 copies)
4790 - Dr. M. Lampe
4790 - Dr. W. M. Manheimer
6603S- Dr. W. W. Zachary
6650 - Dr. L. Cohen
6656 - Dr. N. Seeman
6805 - Dr. S. Y. Ahn
6805 - Dr. A. Ganguly
6805 - Dr. N. R. Vanderplaats
6850 - Dr. L. R. Whicker
6875 - Dr. R. Wagner

On Site Contractors:

Code 4740 - Dr. J. M. Baird (B-K Dynamics)
4740 - Dr. L. Barnett (B-K Dynamics)
4740 - Dr. D. Dialetis (SAI)
4740 - Dr. Y. Y. Lau (SAI)
4740 - Dr. J. S. Silverstein (HDL)
4790 - Dr. A. T. Drobot (SAI)
4790 - Dr. C. M. Tang (JAYCOR)
4790 - Dr. J. Vomvoridis (JAYCOR)(50 copies)
4790 - Dr. H. Freund (SAI)

* Every name listed on distribution gets one copy except for those where extra copies are noted.

Dr. Tony Armstrong
SAI, Inc.
P. O. Box 2351
La Jolla, CA 92038

Dr. Robert Behringer
ONR
1030 E. Green
Pasadena, CA 91106

Dr. G. Bekefi (5 copies)
Massachusetts Institute of Technology
Bldg. 26
Cambridge, MA 02139

Dr. Arden Bement (2 copies)
Deputy Under Secretary of
Defense for R&AT
Room 3E114, The Pentagon
Washington, D.C. 20301

Dr. T. Berlincourt
Code 420
Office of Naval Research
Arlington, VA 22217

Dr. I. B. Bernstein (2 copies)
Yale University
Mason Laboratory
400 Temple Street
New Haven, CT 06520

Dr. Fred Burskirk
Physics Department
Naval Postgraduate School
Monterey, CA 93940

Dr. K. J. Button
Massachusetts Institute of Technology
Francis Bitter National Magnet
Laboratory
Cambridge, MA 02139

Dr. Gregory Canavan
Director, Office of Inertial Fusion
U. S. Department of Energy
M.S. C404
Washington, D.C. 20545

Dr. C. D. Cantrell
T-DOT, MS210
Los Alamos Scientific Laboratory
Los Alamos, NM 87545

Dr. Weng Chow
Optical Sciences Center
University of Arizona
Tucson, AZ 85721

Dr. Peter Clark
TRW, Building R-1, Room 1096
One Space Park
Redondo Beach, CA 90278

Dr. Robert Clark
P. O. Box 1925
Washington, D.C. 20013

Dr. William Colson
Quantum Institute
Univ. of California at Santa Barbara
Santa Barbara, CA 93106

Dr. William Condell
Code 421
Office of Naval Research
Arlington, VA 22217

Dr. Richard Cooper
Los Alamos Scientific Laboratory
P. O. Box 1663
Los Alamos, NM 87545

Cmdr. Robert Cronin
NFOIO Detachment, Suitland
4301 Suitland Road
Washington, D.C. 20390

Dr. R. Davidson (5 copies)
Plasma Fusion Center
Massachusetts Institute of Technology
Cambridge, MA 02139

Dr. John Dawson (2 copies)
Physics Department
University of California
Los Angeles, CA 90024

Defense Technical Information Center
(12 copies)
Cameron Station
5010 Duke Street
Alexandria, VA 22313

Dr. Francesco De Martini
Instituto de Fiscia
"G. Marconi" Univ.
Piazzo delle Science, 5
ROMA00185 ITALY

Prof. P. Diament
Columbia University
Dept. of Electrical Engineering
New York, NY 10027

Prof. H. J. Doucet (5 copies)
Ecole Polytechnique
91128 Palaiseau
Paris, France

Dr. John Elgin (2 copies)
Imperial College
Dept. of Physics (Optics)
London SWF, England

Dr. David D. Elliott
SRI International
333 Ravenswood Avenue
Menlo Park, CA 94025

Dr. Norval Fortson
Department of Physics
University of Washington
Seattle, WA 98195

Director (2 copies)
National Security Agency
Fort Meade, MD 20755
ATTN: Mr. Richard Foss, A42

Dr. Robert Fossum, Director
(2 copies)
DARPA
1400 Wilson Boulevard
Arlington, VA 22209

Dr. Edward A. Frieman
Director, Office of Energy Research
U. S. Department of Energy
M.S. 6E084
Washington, D.C. 20585

Dr. George Gamota (3 copies)
OUSDRE (R&AT)
Room 3D1067, The Pentagon
Washington, D.C. 20301

Dr. Richard L. Garwin
IBM, T. J. Watson Research Center
P. O. Box 218
Yorktown Heights, NY 10598

Dr. Edward T. Gerry, President
W. J. Schafer Associates, Inc.
1901 N. Fort Myer Drive
Arlington, VA 22209

Dr. Avraham Gover
Tel Aviv University
Fac. of Engineering
Tel Aviv, ISRAEL

Dr. A. H. Guenter
Chief Scientist
Air Force Weapons Laboratory
Kirtland AFB, NM 87117

Mr. Donald L. Haas, Director
DARPA/STO
1400 Wilson Boulevard
Arlington, VA 22209

Dr. P. Hammerling
La Jolla Institute
P. O. Box 1434
La Jolla, CA 92038

Director
National Security Agency
Fort Meade, MD 20755
ATTN: Mr. Thomas Handel, A243

Dr. William Happer
560 Riverside Drive
New York City, NY 10027

Dr. Robert J. Hermann
Assistant Secretary of the
Air Force (RD&L)
Room 4E856, The Pentagon
Washington, D.C. 20330

Dr. Rod Hiddleston
KMS Fusion
Ann Arbor, MI 48106

Dr. J. L. Hirshfield (2 copies)
Yale University
Mason Laboratory
400 Temple Street
New Haven, CT 06520

Dr. R. Hofland
Aerospace Corp.
P. O. Box 92957
Los Angeles, CA 90009

Dr. Benjamin Huberman
Associate Director, OSTP
Room 476, Old Executive Office Bldg.
Washington, D.C. 20506

Dr. S. F. Jacobs
Optical Sciences Center
University of Arizona
Tucson, AZ 85721

Dr. Howard Jory (3 copies)
Varian Associates, Bldg. 1
611 Hansen Way
Palo Alto, CA 94303

Mr. Eugene Kopf
Principal Deputy Assistant
Secretary of the Air Force (RD&L)
Room 4E964, The Pentagon
Washington, D.C. 20330

Prof. N. M. Kroll
La Jolla Institutes
P. O. Box 1434
La Jolla, CA 92038

Dr. Tom Kuper
Optical Sciences Center
University of Arizona
Tucson, AZ 85721

Dr. Willis Lamb
Optical Sciences Center
University of Arizona
Tucson, AZ 85721

Mr. Mike Lavan
BMDATC-O
ATTN: ATC-O
P. O. Box 1500
Huntsville, AL 35807

Dr. John D. Lawson (2 copies)
Rutherford High Energy Lab
Chilton
Didcot, Oxon OX11 OOX
ENGLAND

Mr. Ray Leadabrand
SRI International
333 Ravenswood Avenue
Menlo Park, CA 94025

Mr. Barry Leven
NISC/Code 20
4301 Suitland Road
Washington, D.C. 20390

Dr. Donald M. LeVine (3 copies)
SRI International
1611 N. Kent Street
Arlington, VA 22209

Dr. Anthony T. Lin
University of California
Los Angeles, CA 90024

Director (2 copies)
National Security Agency
Fort Meade, MD 20755
ATTN: Mr. Robert Madden, R/SA

Dr. Joseph Mangano
DARPA
1400 Wilson Boulevard
Arlington, VA 22209

Dr. S. A. Mani
W. J. Schafer Associates, Inc.
10 Lakeside Office Park
Wakefield, MA 01880

Dr. Mike Mann
Hughes Aircraft Co.
Laser Systems Div.
Culver City, CA 90230

Dr. T. C. Marshall
Applied Physics Department
Columbia University
New York, NY 10027

Mr. John Meson
DARPA
1400 Wilson Boulevard
Arlington, VA 22209

Dr. Pierre Meystre
Projektgruppe fur Laserforschung
Max Planck Gesellschaft
Garching, Munich GERMANY

Dr. Gerald T. Moore
Optical Sciences Center
University of Arizona
Tucson, AZ 85721

Dr. Philip Morton
Stanford Linear Accelerator Center
P. O. Box 4349
Stanford, CA 94305

Dr. Jesper Munch
TRW
One Space Park
Redondo Beach, CA 90278

Dr. George Neil
TRW
One Space Park
Redondo Beach, CA 90278

Dr. Kelvin Neil
Lawrence Livermore Laboratory
Code L-321, P. O. Box 808
Livermore, CA 94550

Dr. Milton L. Noble (2 copies)
General Electric Company
G. E. Electronic Park
Syracuse, NY 13201

Prof. E. Ott (2 copies)
University of Maryland
Dept. of Physics
College Park, Md. 20742

Dr. Richard H. Pantell
Stanford University
Stanford, CA 94305

Dr. Richard M. Patrick
AVCO Everett Research Lab., Inc.
2385 Revere Beach Parkway
Everett, MA 02149

The Honorable William Perry
Under Secretary of Defense (R&E)
Office of the Secretary of Defense
Room 3E1006, The Pentagon
Washington, D.C. 20301

Dr. Alan Pike
DARPA/STO
1400 Wilson Boulevard
Arlington, VA 22209

Dr. Hersch Pilloff
Code 421
Office of Naval Research
Arlington, VA 22217

Dr. Charles Planner
Rutherford High Energy Lab
Chilton
Didcot, Oxon, OX11 0QX,
ENGLAND

Dr. Michal Poole
Daresbury Nuclear Physics Lab.
Daresbury, Warrington
Cheshire WA4 4AD
ENGLAND

Dr. Don Prosnitz
Lawrence Livermore Laboratory
Livermore, CA. 94550

Dr. D. A. Reilly
AVCO Everett Research Lab.
Everett, MA 02149

Dr. James P. Reilly
W. J. Schafer Associates, Inc.
10 Lakeside Office Park
Wakefield, MA 01880

Dr. A. Renieri
C.N.E.N.
Div. Nuove Attivita
Dentro di Frascatti
Frascatti, Rome
ITALY

Dr. Daniel N. Rogovin
SAI
P. O. Box 2351
La Jolla, CA 92038

Dr. Michael Rosenbluh
MIT - Magnet Lab.
Cambridge, MA 02139

Dr. Marshall N. Rosenbluth
Institute for Advanced Study
Princeton, NJ 08540

Dr. Eugene Ruane (2 copies)
P. O. Box 1925
Washington, D.C. 20013

Dr. Antonio Sanchez
MIT/Lincoln Laboratory
Room B231
P. O. Box 73
Lexington, MA 02173

Prof. S. P. Schlesinger
Columbia University
Dept. of Electrical Engineering
New York, NY 10027

Dr. Howard Schlossberg
AFOSR
Bolling AFB
Washington, D.C. 20332

Dr. Stanley Schneider
Rotodyne Corporation
26628 Fond Du Lac Road
Palos Verdes Peninsula, CA 90274

Dr. Marlan O. Scully
Optical Sciences Center
University of Arizona
Tucson, AZ 85721

Dr. Robert Sepucha
DARPA/STO
1400 Wilson Boulevard
Arlington, VA 22209

Dr. A. M. Sessler
Lawrence Berkeley Laboratory
University of California
1 Cyclotron Road
Berkeley, CA 94720

Dr. Earl D. Shaw
Bell Labs
600 Mountain Avenue
Murray Hill, NJ 07974

Dr. Chan-Ching Shih
R&D Associates
P. O. Box 9695
Marina del Rey, CA 92091

Dr. Kenneth Smith
Physical Dynamics, Inc.
P. O. Box 556
La Jolla, CA 92038

Mr. Todd Smith
Hansen Labs
Stanford University
Stanford, CA 94305

Dr. Joel A. Snow
Senior Technical Advisor
Office of Energy Research
U. S. Department of Energy, M.S. E084
Washington, D.C. 20585

Mrs. Alma Spring
DARPA/Administration
1400 Wilson Boulevard
Arlington, VA 22209

SRI/MP Reports Area G037 (2 copies)
333 Ravenswood Avenue
Menlo Park, CA 94025
ATTN: D. Leitner

Dr. Abraham Szoke
Lawrence Livermore Laboratory
MS L-470, P. O. Box 808
Livermore, CA 94550

Dr. Milan Tekula
AVCO Everett Research Lab.
2385 Revere Beach Parkway
Everett, MA 02149

Dr. R. Temkin (2 copies)
Plasma Fusion Center
Massachusetts Institute of Technology
Cambridge, MA 02139

Dr. John E. Walsh
Department of Physics
Dartmouth College
Hanover, NH 03755

Dr. Wasneski (2 copies)
Naval Air Systems Command
Department of the Navy
Washington, D.C. 20350

Lt. Col. W. Whitaker
Defense Advanced Research Projects
Agency
1400 Wilson Boulevard
Arlington, VA 22209

Ms. Bettie Wilcox
Lawrence Livermore Laboratory
ATTN: Tech. Info. Dept. L-3
P. O. Box 808
Livermore, CA 94550

Dr. A. Yariv
California Institute of Tech.
Pasadena, CA 91125


END
DATE
FILMED
1 - 8
DTIC